GEORGIA INSTITUTE OF TECHNOLOGY — OFFICE OF CONTRACT ADMINISTRATION

PROJECT ADMINISTRATION DATA SHEET

[X] ORIGINAL [ ] REVISION NO. _____

Project No. G-35-681 (R6199-0A0) GTRC/~~GIT~~ DATE 9 / 11 / 86

Project Director: D.D. Davis & R.E. Stickel School/~~Lab~~ Geo Sci

Sponsor: National Science Foundation

Type Agreement: Grant No. ATM - 8610236

Award Period: From 6/15/86 To 2/29/89 * (Performance) 5/31/88 (Reports)

Sponsor Amount:

	This Change	Total to Date
Estimated:	$	$ 286,931 **
Funded:	$	$ 136,931

Cost Sharing Amount: $ _____ Cost Sharing No: G-35-372

Title: A Vacuum - Ultraviolet Photofragmentation/Laser-induced Florescence Sensor For Measurement of Atmospheric Trace Gases

ADMINISTRATIVE DATA OCA Contact John B. Schonk X-4820

1) Sponsor Technical Contact:

Jarvis L. Moyers
National Science Foundation
AAEO/ATM
Washington, D.C. 20550
202/357-9657

2) Sponsor Admin/Contractual Matters:

Stanley C. Dobson
National Science Foundation
DGC/AAEO
Washington, D.C. 20550
202/357-9630

Defense Priority Rating: N/A Military Security Classification: N/A

(or) Company/Industrial Proprietary: N/A

RESTRICTIONS

See Attached NSF Supplemental Information Sheet for Additional Requirements.

Travel: Foreign travel must have prior approval – Contact OCA in each case. Domestic travel requires sponsor approval where total will exceed greater of $500 or 125% of approved proposal budget category.

Equipment: Title vests with GIT

COMMENTS:

*Includes a six month unfunded flexibility period.

Preaward costs from 6/15/86 have been approved.

**An additional one year of funding is anticipated for this project

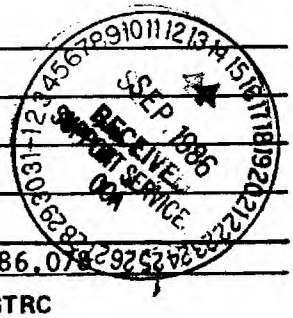

SPONSOR'S I. D. NO. 02.107.000.86.07

COPIES TO:

Project Director
Research Administrative Network
Research Property Management
Accounting
Procurement/GTRI Supply Services
Research Security Services
[redacted]
Research Communications (2)
GTRC
Library
Project File
Other A. Jones

GEORGIA INSTITUTE OF TECHNOLOGY
OFFICE OF CONTRACT ADMINISTRATION

NOTICE OF PROJECT CLOSEOUT

Closeout Notice Date 06/17/91

Project No. G-35-681 Center No. R6199-0A0

Project Director DAVIS D D School/Lab E & A SCI

Sponsor NATL SCIENCE FOUNDATION/GENERAL

Contract/Grant No. ATM-8610236 Contract Entity GTRC

Prime Contract No. _____

Title A VACUUM-ULTRAVIOLET PHOTOFRAG/LASER-INDUCED FLUORESCENCE SENOR FOR MEAS

Effective Completion Date 890228 (Performance) 890531 (Reports)

Closeout Actions Required:	Y/N	Date Submitted
Final Invoice or Copy of Final Invoice	N	
Final Report of Inventions and/or Subcontracts	Y	910610
Government Property Inventory & Related Certificate	Y	
Classified Material Certificate	N	
Release and Assignment	N	
Other _____	N	

Comments _____

Subproject Under Main Project No. _____

Continues Project No. _____

Distribution Required:

Project Director	Y
Administrative Network Representative	Y
GTRI Accounting/Grants and Contracts	Y
Procurement/Supply Services	Y
Research Property Management	Y
Research Security Services	N
Reports Coordinator (OCA)	Y
GTRC	Y
Project File	Y
Other _____	N
_____	N

NOTE: Final Patent Questionnaire sent to PDPI

I. PROGRESS REPORT

A. Introduction

Based on the successes achieved with both the TP-LIF NO and UV/PF-LIF NO_2 systems (Bradshaw et al. 1982; Bradshaw et al. 1985; Davis et al. 1987; Sandholm et al. 1987), two years ago the Georgia Tech group proposed to NSF yet a third detection scheme that fell under the heading of multi-photon LIF technology: Vacuum UV/Photofragmentation LIF (VUV/PF-LIF). As shown in Fig. 1 (for the case of the polyatomic species ABC), a key feature of this new methodology is that photofragmentation is achieved in the near vacuum UV. Critical to the tropospheric application of this new approach is the fact that even at wavelengths as short as 193 nm, laser beams can be propagated one to two meters in air without major losses in energy. This means that numerous atmospheric trace gases which either have low or non-existent absorption cross sections in the UV can potentially be detected in the near vacuum UV where typical cross sections are in the range of $10^{-17}cm^2$.

However, even though the above cited absorption data provides one with good reason for optimism in the detection of polyatomic species, this new technique, unlike the UV/PF-LIF system, does not satisfy the condition of $\lambda_3 < \lambda_2$ and λ_1. Thus, the white background fluorescence noise from the λ_1 VUV laser must be dealt with. As shown in Fig. 1, this problem can be handled if the lifetime of the photofragment species, AB^*, is sufficiently long lived (as dictated by its natural lifetime, quenching by atmospheric gases or reaction with other species) to permit a time delay between the firing of the λ_1 and λ_2 lasers. By using appropriately adjusted delay times, the only remaining condition that must be met is that $\lambda_3 < \lambda_2$.

Two years ago we proposed that at least four molecules were likely to satisfy most of the conditions required of a VUV/PF-LIF system: NH_3, CS_2, SO_2,

Fig. 1

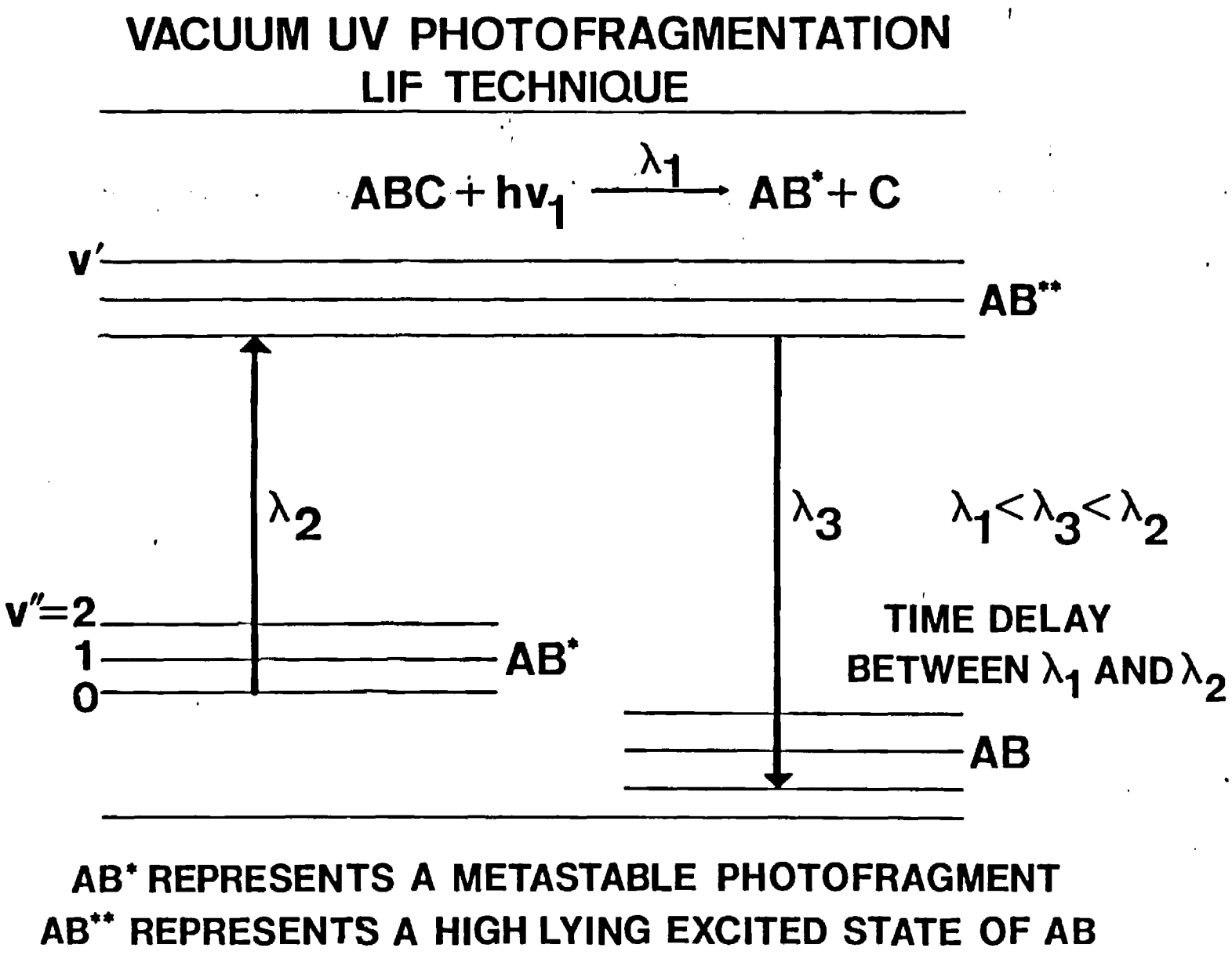
VACUUM UV PHOTOFRAGMENTATION
LIF TECHNIQUE
ABC + hν1 → λ1 AB* + C
v'
AB**
λ2
λ3
λ1<λ3<λ2
v''=2
1
0
AB*
TIME DELAY
BETWEEN λ1 AND λ2
AB
AB* REPRESENTS A METASTABLE PHOTOFRAGMENT
AB** REPRESENTS A HIGH LYING EXCITED STATE OF AB

and H_2S. Of these possibilities, based on the availability of spectroscopic/photodynamic data as well as scientific need, we selected NH_3 as our first test molecule for checking out the VUV/PF-LIF approach.

The detection scheme for NH_3 is that given below:

$NH_3 + 2h\nu_1$ (193 nm) $\rightarrow$ NH ($b^1\Sigma^+$) + H_2 (or 2H)

NH ($b^1\Sigma$,v"=0) + $h\nu_2$ (450 nm) $\rightarrow$ NH ($c^1\Pi$,v'=0)

NH ($c^1\Pi$,v'=0) $\rightarrow$ NH ($a^1\Delta$,v"=0) + $h\nu_3$ (326 nm).

The final hardware configuration developed for the NH_3 system during the first two years of our program is shown in Fig. 2.

Suffice it to say, the progress made on the NH_3 system during the first two years clearly demonstrated: (1) proof-of-concept in applying the VUV/PF-LIF technique to the atmospheric detection of NH_3; (2) provided a sufficient data base from which one could readily conclude that the necessary sensitivity for routine measurement of NH_3, under virtually any set of environmental conditions, was available; (3) demonstrated that the technique was free of any major interferences such as those from organic amines; and (4), tests were performed that showed that one of the more difficult problems in making field measurements of NH_3, wall memory problems, was one that could be overcome in the VUV/PF-LIF system. The solution to the latter problem involved both the proper selection of materials for sampling lines and the fluorescence chamber as well as the use of exceptionally high sampling flow rates.

Thus, in going into the third year of this program, we had reason to feel optimistic. The major tasks before us were: (1) that of optimizing the system for making routine field measurements; (2) establishing an improved theoretical base for the system, especially as related to quenching cross-sections for the NH'b state; and (3) that of initiating the first of a series of tropospheric field measurements of NH_3 and related chemical variables. Each of these areas of activity has been further expanded on in the text that follows.

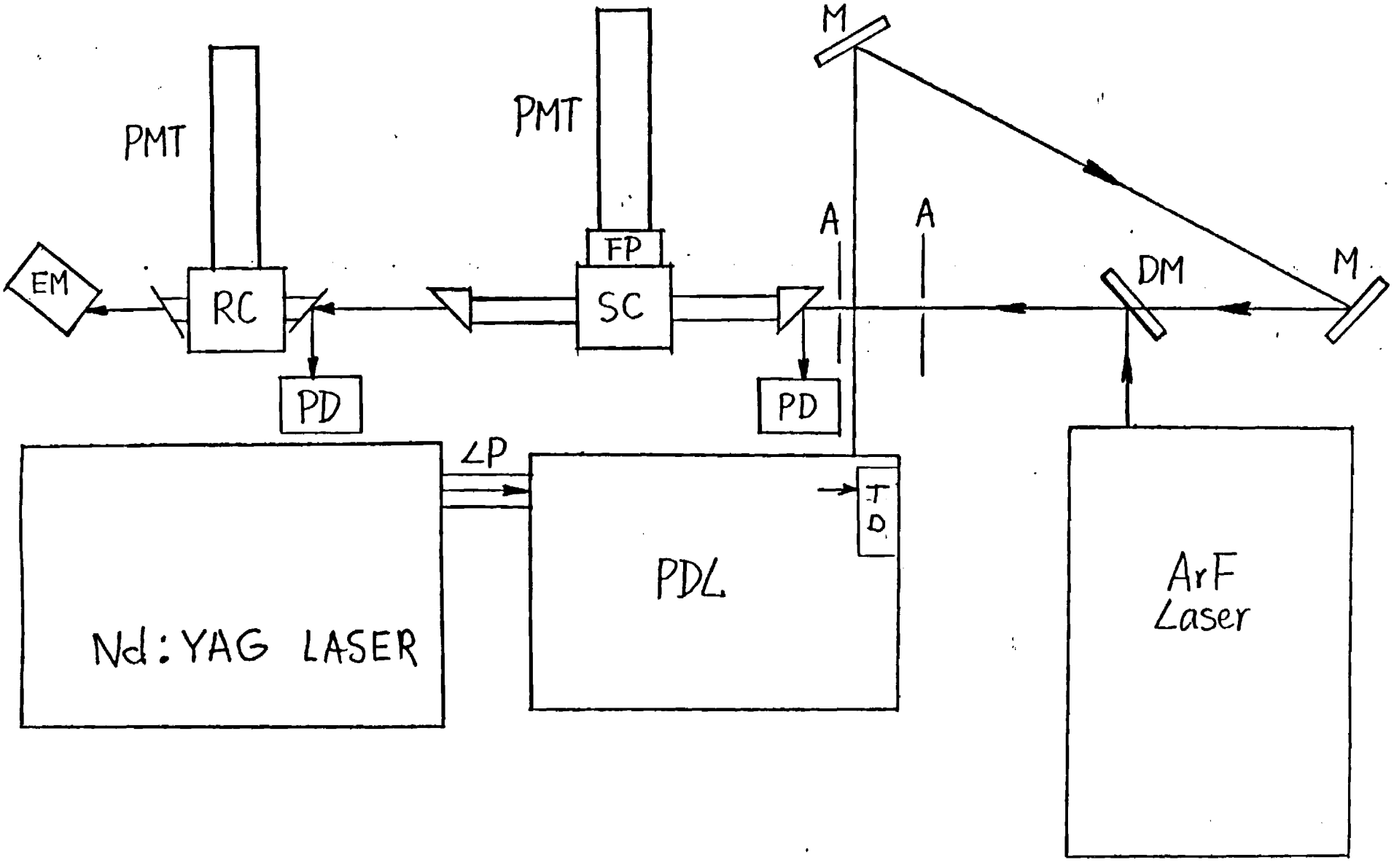

Fig. 2 - VUV/PF-LIF HARDWARE CONFIGURATION IV: CURRENT NH_3 DETECTION SYSTEM

(LP) Laser Pipe; (TD) Fast Timing Diode; (M) Mirror; (DM) Dichroic Mirror; (A) Aperture; (PD) Photodiode; (SC) Sample Cell; (FP) Filter Pack; (PMT) Photomultiplier Tube; (RC) Reference Chamber; (EM) Energy Monitor.

B. Optimization Tasks

There are four areas in which extensive time was invested in the proto-type VUV/PF-LIF system during the 3rd year: (1) calibration exercises; (2) noise reduction tests; (3) sampling hysteresis; and (4) sensitivity analysis.

(1) Calibration Exercises

In earlier efforts to calibrate the NH_3 system by our group, a concentration range of 1 ppb to 120 ppmv was covered, i.e. a dynamic range of over 10^5. A least squares fit of these earlier results (e.g. log signal vs. log NH_3) gave a slope of .85 ± .2; however, the scatter in these data was shown to be substantially greater than that needed for a reliable NH_3 field sampling system. This was especially true for levels at or below 50 ppbv where for some individual data points the deviation from the best-fit least squares line approached nearly a factor of ten. In addition, the lowest NH_3 concentration at which a calibration had been performed was ~ 1 ppbv.

Upon completing a thorough examination of this system, three problem areas were identified as being the potential cause of the large uncertainties in these earlier calibration curves: (a) the presence of extensive secondary chemistry in the NH_3 reference chamber; (b) the presence of teflon tubing in the calibration system; and (c) the need for long equilibration times in the dynamic-dilution calibration system when changing NH_3 concentration levels.

Concerning the first problem area, initially high levels of NH_3 (100 ppmv) were used in the presence of air as the reference cell gas mixture. As a result, large amounts of O_3, NH_2 radicals, as well as other radical species were reacting very rapidly with the key species NH'b. Thus, the reference cell did not track the ambient cell as well as it should have with changes in the λ_1 and

λ_2 laser energy densities, as well as with changes in the λ_2 delay time. The latter problem was corrected by reducing the concentration of NH_3 in the reference cell to ~ 2 ppmv and by diluting the NH_3 calibration mix with pure N_2 rather than air. The second problem area simply involved the removal of teflon tubing and replacing it wherever possible with passivated nickel tubing or some other non-porous tubing. The calibration system problem was resolved by maintaining a fixed output of NH_3 from the dynamic dilution system. Thus, rather than continually changing the concentration level of NH_3 generated within the calibration source, we now maintain a fixed NH_3 level. The fixed NH_3 concentration is then adjusted to the final calibration level in the ambient air sampling line by its addition to the sampling line through one of four different rotometers. Which rotometer is selected therefore determines what fraction of the total cal-gas mixture is injected into the sampled gas stream.

As a result of making the above changes, we can now generate calibration curves as shown in Figs. 3 and 4, covering the critical atmospheric concentration range of 63 pptv up to 12 ppbv. It will be noticed that a linear regression analysis of these data gives a log-log slope of .98 ± .05. The average deviation of the linear plot is ± 18%. It is thus apparent that a substantial improvement in both sensitivity and precision has been achieved over the proto-type NH_3 system.

(2) Noise Reduction Tests

One of the early disappointments in the proto-type VUV/PF-LIF NH_3 system was our discovering that the noise from the 193 excimer laser was much higher than our earlier theoretical calculations would have suggested. Thus, instead of being able to work at delay times of a 1μs or less, we were forced to work at delay times of nearly 5μs. The 5μs delay time not only results in the direct

Fig. 3 CALIBRATION CURVE

of 4/20/87

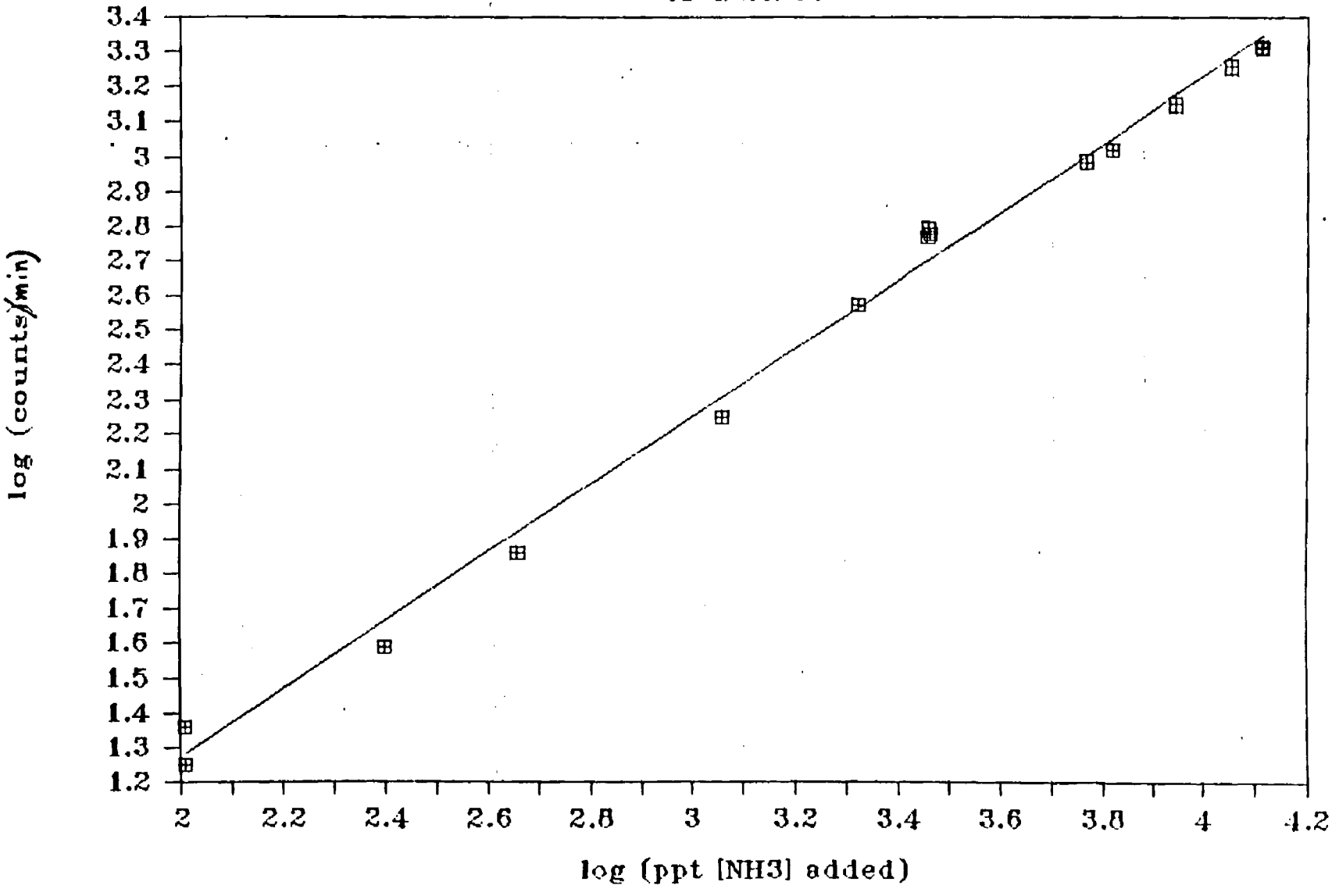

Fig. 4 CALIBRATION CURVE

of 4/20/87

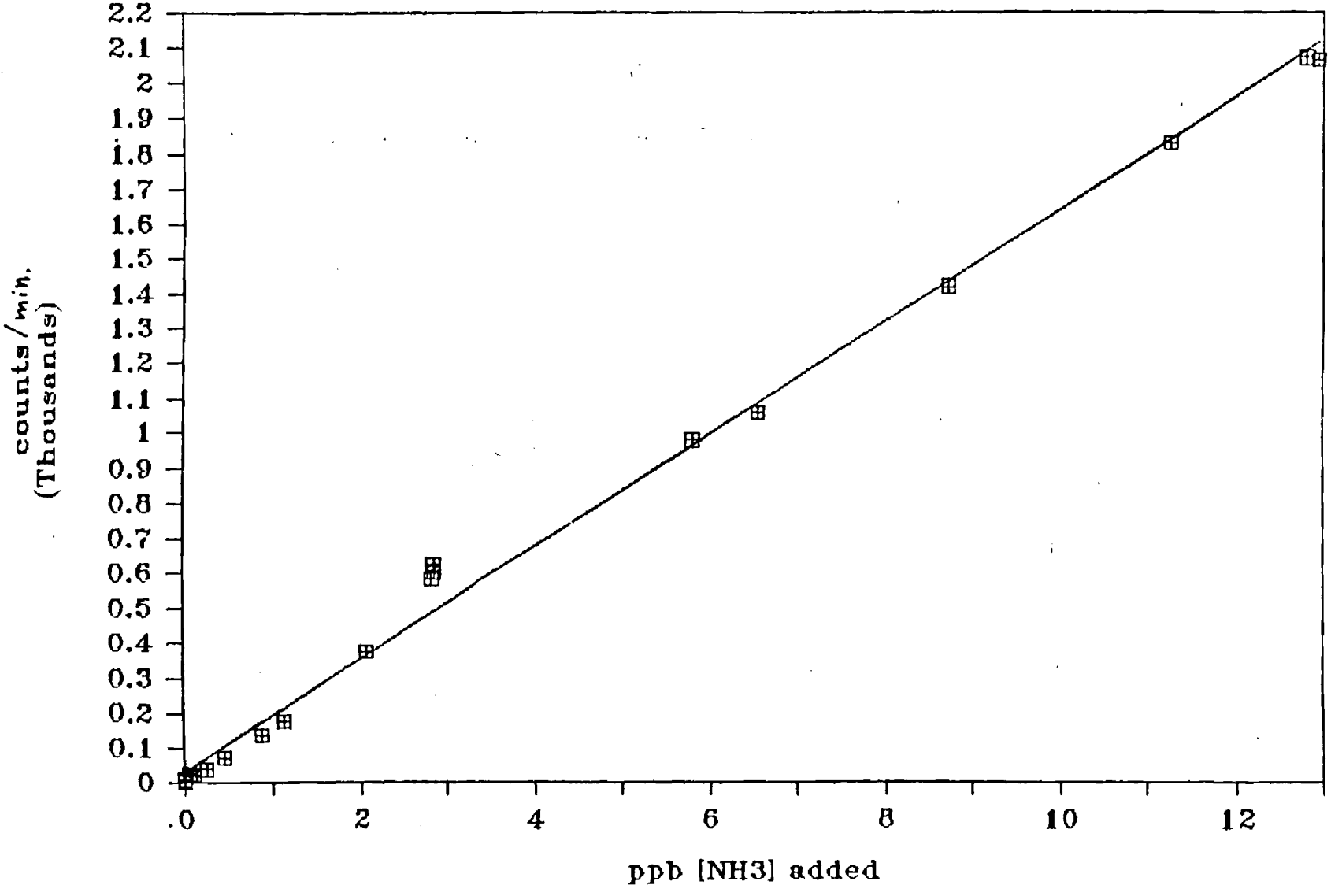

loss of signal due to quenching of the NH'c electronic state, but also can cause an even further decrease in signal in the presence of high concentrations of H_2O due to the quenching and/or reactions of the NH'b state by H_2O. Through the use of soft focusing techniques, in conjunction with the insertion of additional apperatures between the 193 excimer and the ambient fluorescence cell, we have been able to reduce the noise level by over a factor of five. This together with other electronic changes, now allow for the use of 2 to 3μs delay times. Thus, a substantial enhancement has been gained in sensitivity for detection of NH_3 especially under high water conditions.

At this point we believe that still shorter times could be achieved in this system. One possibility proposed in our original document was the use of a microchannel plate PMT rather than a conventional dynode chain PMT. The major difference between these two systems is that the microchannel plate PMT is so constructed as to permit much faster gating "on" an "off" without the generation of electrical transients that can be picked up and amplified by pulse counting electronics. Tests now completed with this device did indeed show that gating of this PMT at times as short as .5μs was quite tractable; however, the noise profile, which should have been representative of only the white fluorescence noise from the 193 nm laser, was not appreciably different from that extrapolated from the currently employeed R331 dynode chain PMT. In the case of the microchannel plate PMT, we were monitoring the true fluorescence noise from the 193 laser and these results suggest that delay times as short as 1μs should be usable in the VUV/PF-LIF system in the near future. This should significantly improve the projected performance for the detection of SO_2 and CS_2 via the VUV-PF-LIF method but result in only modest improvements in the detection sensitivity for NH_3 and H_2S.

(3) Sampling Hysteresis

Although earlier sampling hysteresis tests in our lab using the proto-type NH_3 system were encouraging, the conditions under which these tests were carried

out did not represent conditions that were directly amenable to field sampling conditions. In the earlier tests, the calibration system both before an NH_3 injection and after terminating an NH_3 injection was phyically disconnected from the main sampling line to the cell. Under normal field sampling conditions the calibration system would remain mechanically coupled to the main sampling line and would be isolated from the main line via a shut off valve.

Shown in Figs. 5 and 6 are injection tests involving 2.5 and - 10.5 ppbv, of NH_3, respectively. In these tests the air flow was 150 ℓ/min. At no time during these tests was the calibration system physically disconnected from the main sampling line, i.e. isolation was achieved by means of a rotometer shut off valve. In both cases it can be seen that the rise and fall time for 90% response was - 1 minute for changes in the NH_3 level of 10 or greater. However, a further qualifier concerning the data set shown in Figs. 5 and 6 involves the fact that the length of the sampling line in the aforementioned tests was only a few inches in length at the point of injection. As will be noted later in the text, for the field measurement study on the Georgia Tech campus, we used 28' of 1 1/4" I.D. pyrex tubing as the sampling line. In the latter case, it will be seen that the 90% response times are closer to - 5 min. for a 10 fold change in concentration levels. (Normally for ground based or airborne sampling the sampling line length would be closer to 7 to 8', and we would predict an - 2 min. recovery time.) Overall, however, this modified NH_3 system appears to have minimal hysteresis problems.

(4) Sensitivity Analysis

Based on the improvements made to the proto-type VUV-PF/LIF NH_3system during the third year, we now believe we can predict the field performance characteristics of this system under a wide range of atmospheric conditions. These estimates are shown in Table I for conditions involving 10 mJ of 193 nm energy (currently on hand) as well as 35 mJ of 193 nm energy which is baed on

Fig. 5 [NH3] "SPIKE" RESPONSE

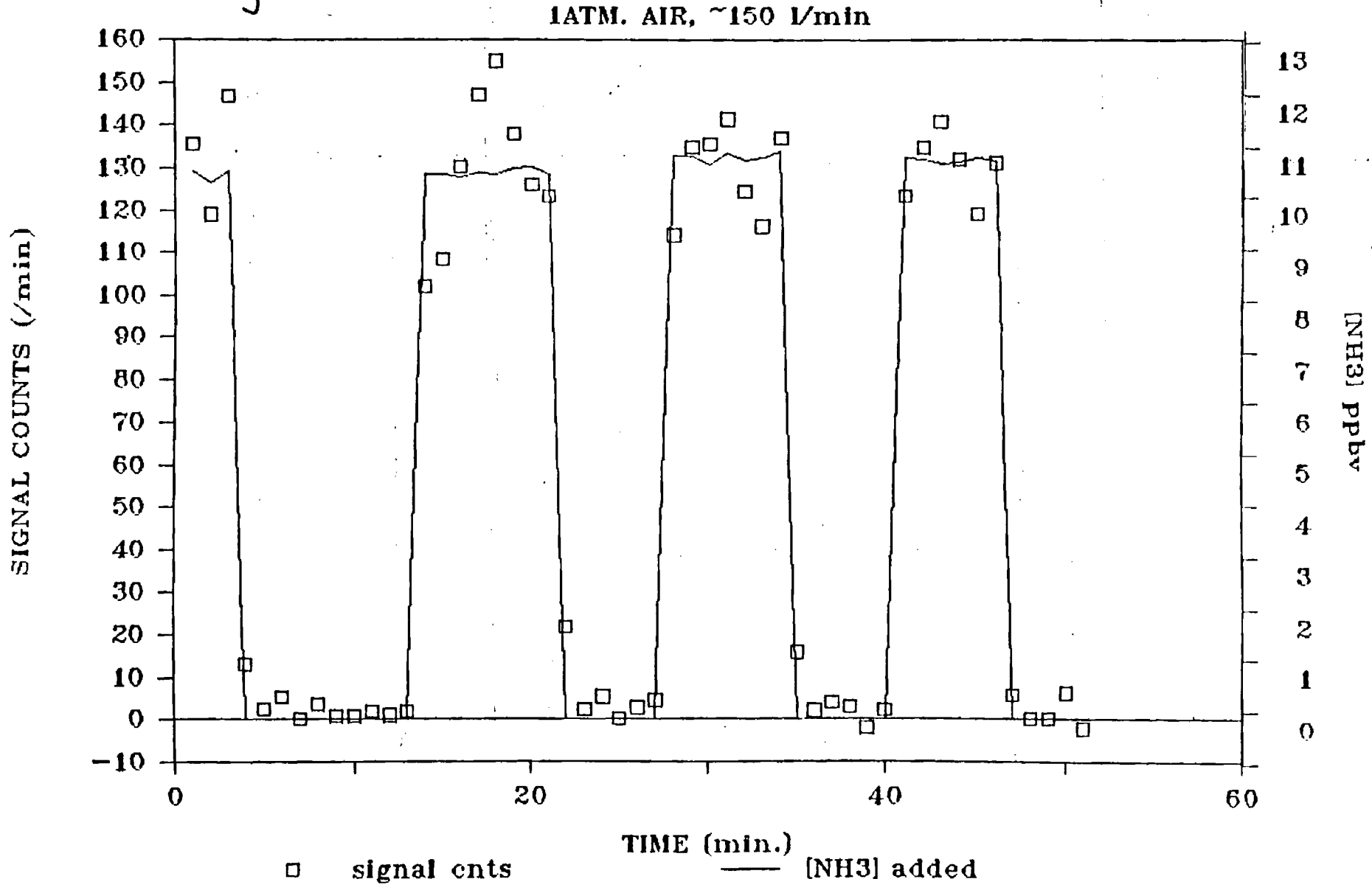

Fig.6 [NH3] "SPIKE" RESPONSE

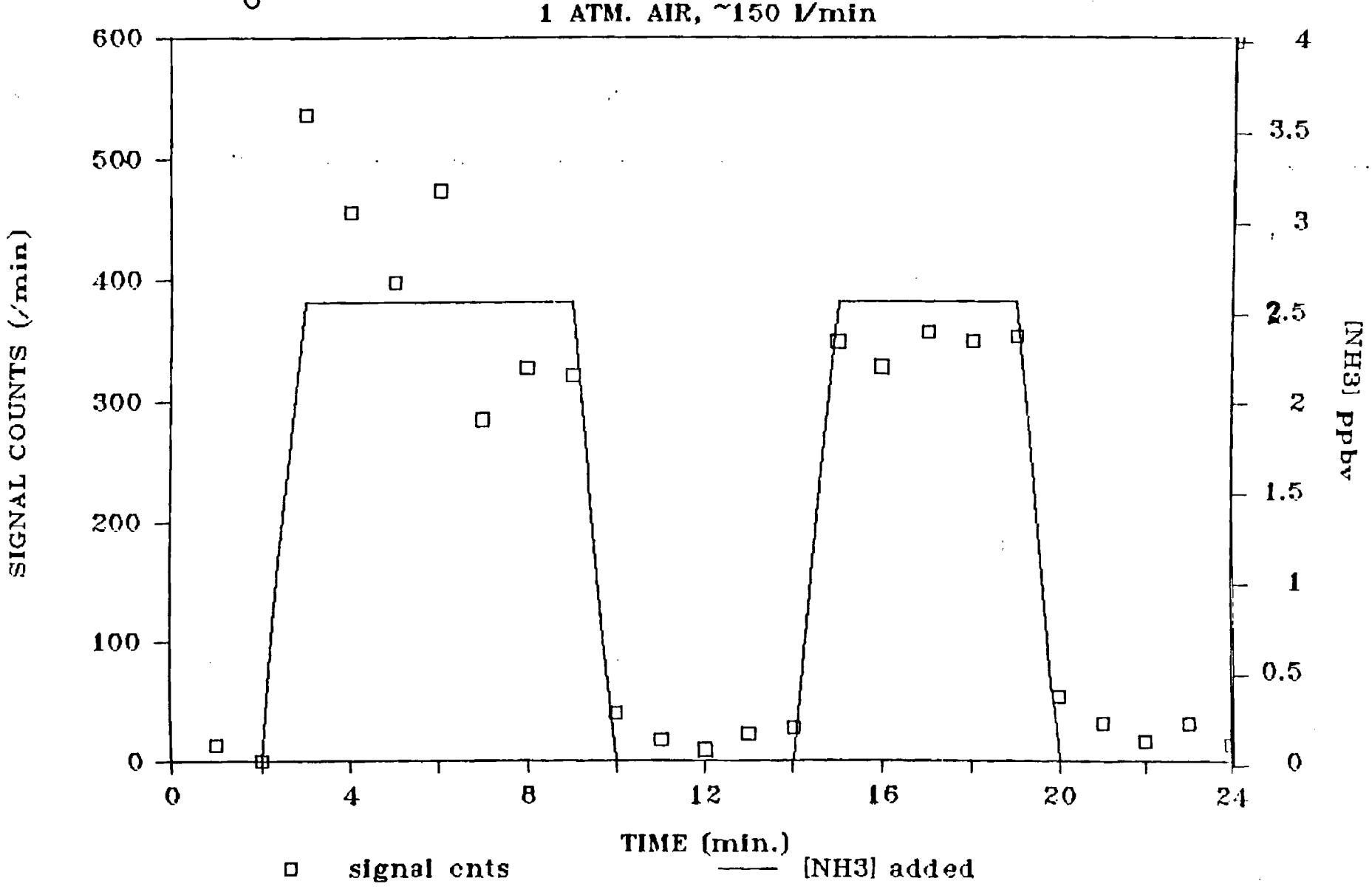

the up-grading of our existing EXC-I laser (for ArF operation) to an EXC-II level performance. (This up-grading has already been done for the case of XeF gas operations.) Yet another critical system parameter upon which these estimates are based is the use of a λ_2 delay time of no more than 3 μs. As noted earlier in the text, this operating mode now has been fully tested.

Table I

Operational VUV/PF-LIF NH_3 Detection System

Sampling Conditions	Integ. Time	NH_3 L.O.D.(2σ) E_{193} = 10 mJ (1 PMT)	NH_3 L.O.D.(2σ) E_{193} = 35 mJ (2 PMT's)
12 Torr H_2O (Urban Envir. Grd. Level)	5 min.	50 pptv	10 pptv
"	1 min.	110 pptv	21 pptv
12 Torr H_2O (Clean Trop.) Sea Level	5 min.	18 pptv	4 pptv
"	1 min.	38 pptv	9 pptv
<1 Torr H_2O (Clean Trop.) 6 km	5 min.	5 pptv	1.2 pptv
"	1 min.	12 pptv	3 pptv

From Table I, it can be seen that even with the existing 10 mJ (193 nm)/1 PMT NH_3 detection system there is unlikely to be a set of tropospheric conditions in which the VUV/PF-LIF system would not be capable of making reliable NH_3 measurements. With the upgrading of the excimer laser and the addition of one more PMT, 1 minute time resolution should become possible under virtually all conditions. Still further improvements in the L.O.D. for NH_3 could be realized in the case of high levels of atmospheric water by moving the delay time back to ~ 1μs.

C. Quenching Studies

Because of the need to delay the λ_2 laser pulse relative to the firing of the λ_1 laser, the lifetime of the detected photofragment from NH_3, NH'b, is of critical importance in determining the ultimate sensitivity of the VUV/PF-LIF sensor in detecting NH_3 under tropospheric conditions. Earlier, in our renewal proposal (June 1986) we reported results on the quenching of the NH'b species by O_2 and N_2 as well as from air mixtures. These results were in reasonably good agreement with those of Zetzach and Stuhl, 1976. These results therefore confirmed that the quenching of the NH'b state by air presented no difficulties in the detection of NH'b since delay times between the firing of the λ_1 and λ_2 lasers as long as 10μs in air could easily by tolerated without a significant loss in signal strength.

However, a potentially much more sensitive atmospheric species that could effect the lifetime of the NH'b state is H_2O. For example, using the only rate data available involving the interaction* of H_2O with NH'b (i.e. Zetzsch and Stuhl, 1976), $k_{H2O} = 4.9 \times 10^{-13} cm^3$ molec^{-1} s^{-1}), the lifetime of the NH'b species varies from 27μs for conditions of 0°C and 50% relative humidity to as short as 2μs at 30°C and 90% relative humidity. (The latter conditions would be those encountered in a south Georgia marshland during summer months.) Thus, based on this one reported set of H_2O measurements it can be concluded that a significant signal increase could result in the VUV/PF-LIF NH_3 system if the λ_2 delay time of 5μs could be reduced to 2μs. For this reason, we felt it quite important to independently examine the rate coefficient for the process H_2O + NH'b → products. However, to increase our confidence level in any new quenching measurements for the process H_2O + NH'b, it was thought prudent to also examine several other molecules that had been studied by Zetzsch and Stuhl (1976). The list, in this case, included H_2O, H_2, CH_4, C_2H_6, and C_3H_6. The

---

* It is still unknown whether this interaction involves H-atom abstraction or simply quenching of the NH'b state to NH'a.

gases H_2, CH_4, C_2H_6, and C_3H_6 used in this investigation were UHP grade with a stated purity of 99.999%. The HPLC grade H_2O was purchased from Burdick and Jackson. In our experiments, the quenching and/or reaction rate coefficient for the NH'b state was determined from a measurement of the NH'c fluorescence versus delay time. The delay time in this case was that between the firing of 193 nm λ_1 photolysis laser and the 453 nm λ_2 laser, used to excite the NH'b state to the NH'c state. Fluorescence was detected from the transition of NH'c to the NH'a state. Thus, from first order plots of ln (Fluor) versus delay time together with known concentration levels of the quenching and/or reactant gas, the desired rate coefficients could be directly calculated. Typical decay curves are shown in Figs. 7,8,9,and 10. In each of these experiments the diluent gas was ultra high purity N_2 at ~ 1 atm. pressure.

The final results from these experiments, as well as those from Zetzsch and Stuhl (1976) are summarized in Table II.

Fig. 7 H2O "QUENCHING" NH1b

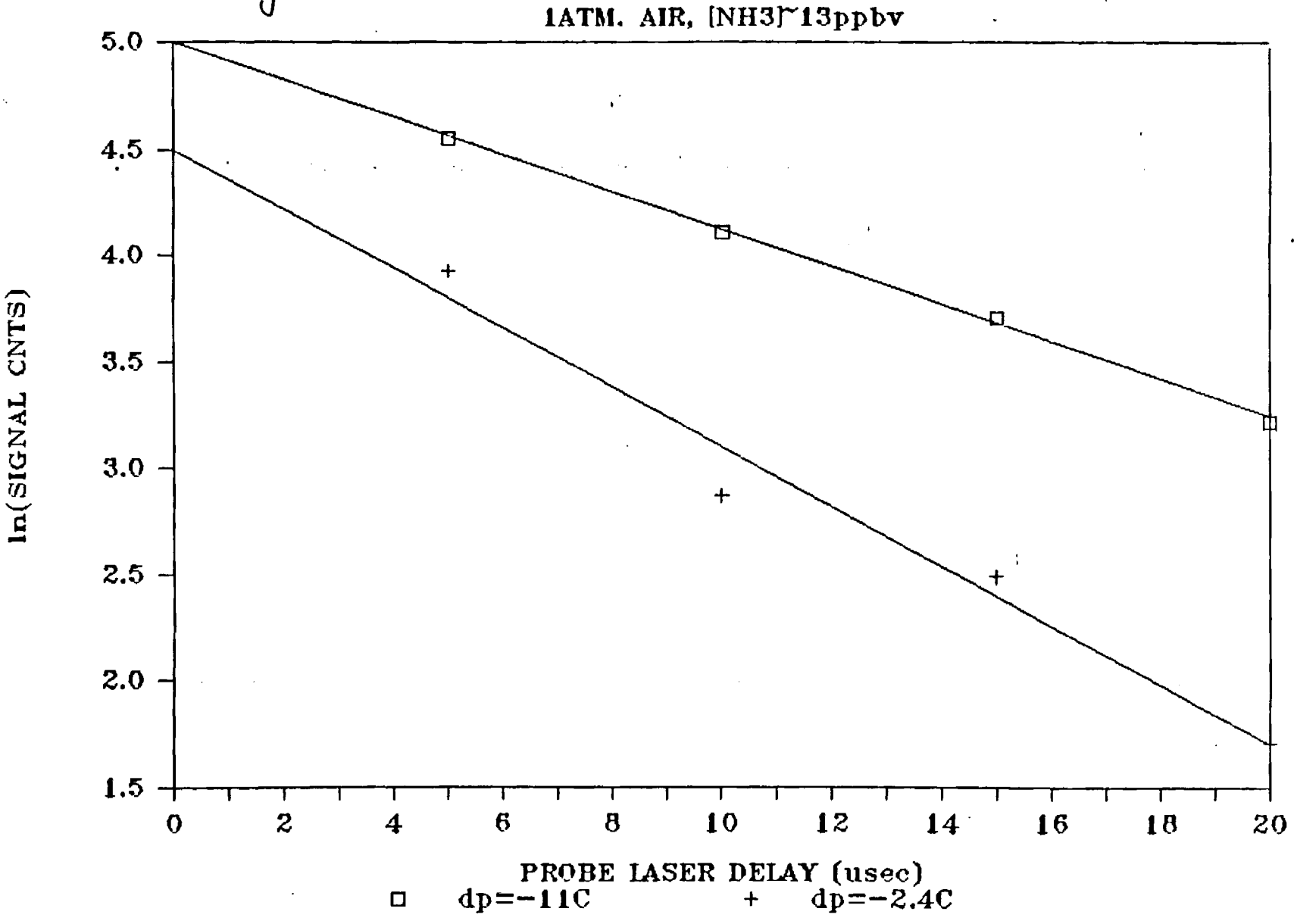

Fig.8 H2O "QUENCHING" NH1b

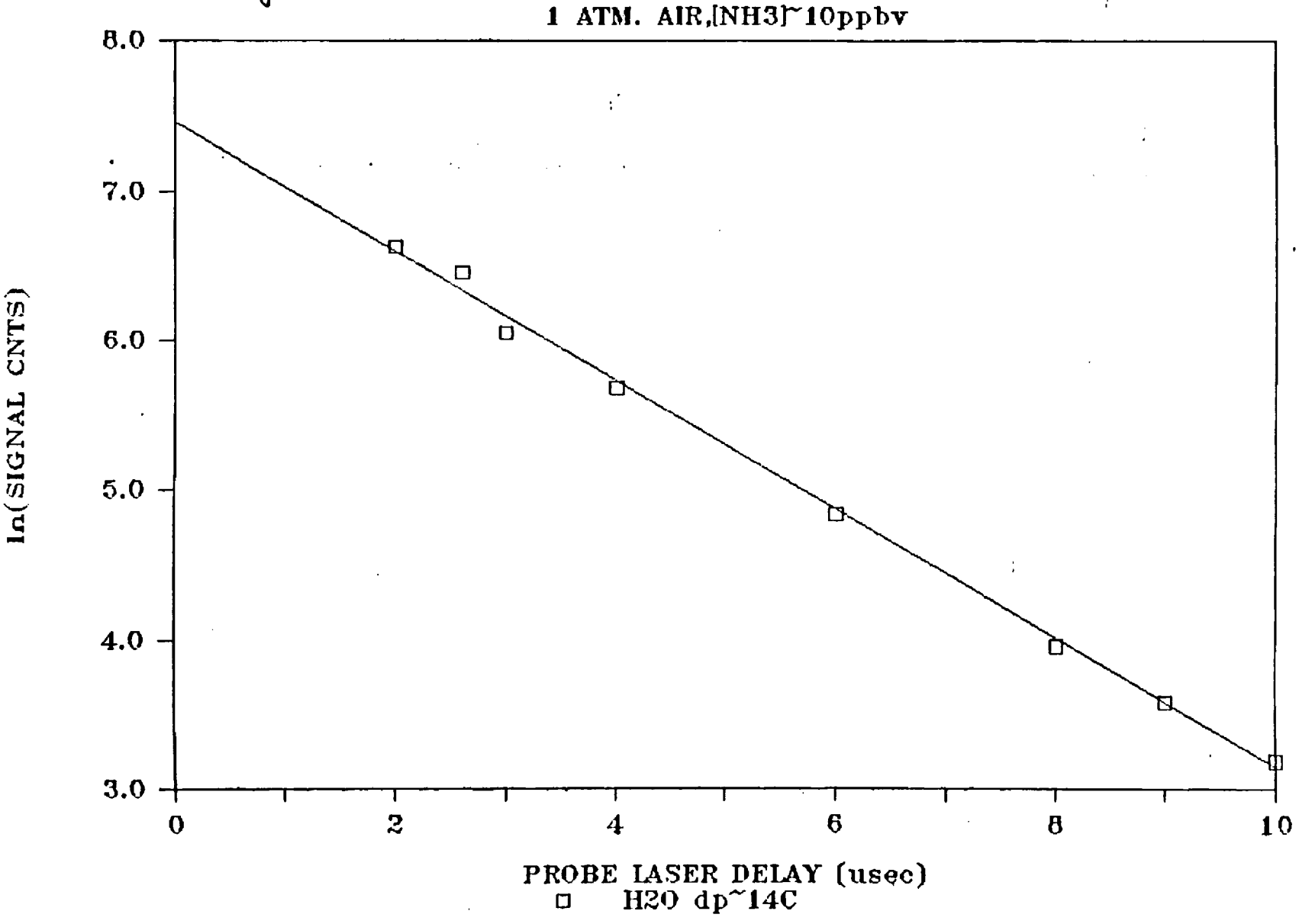

Fig. 9 [M] "QUENCHING" NH1b

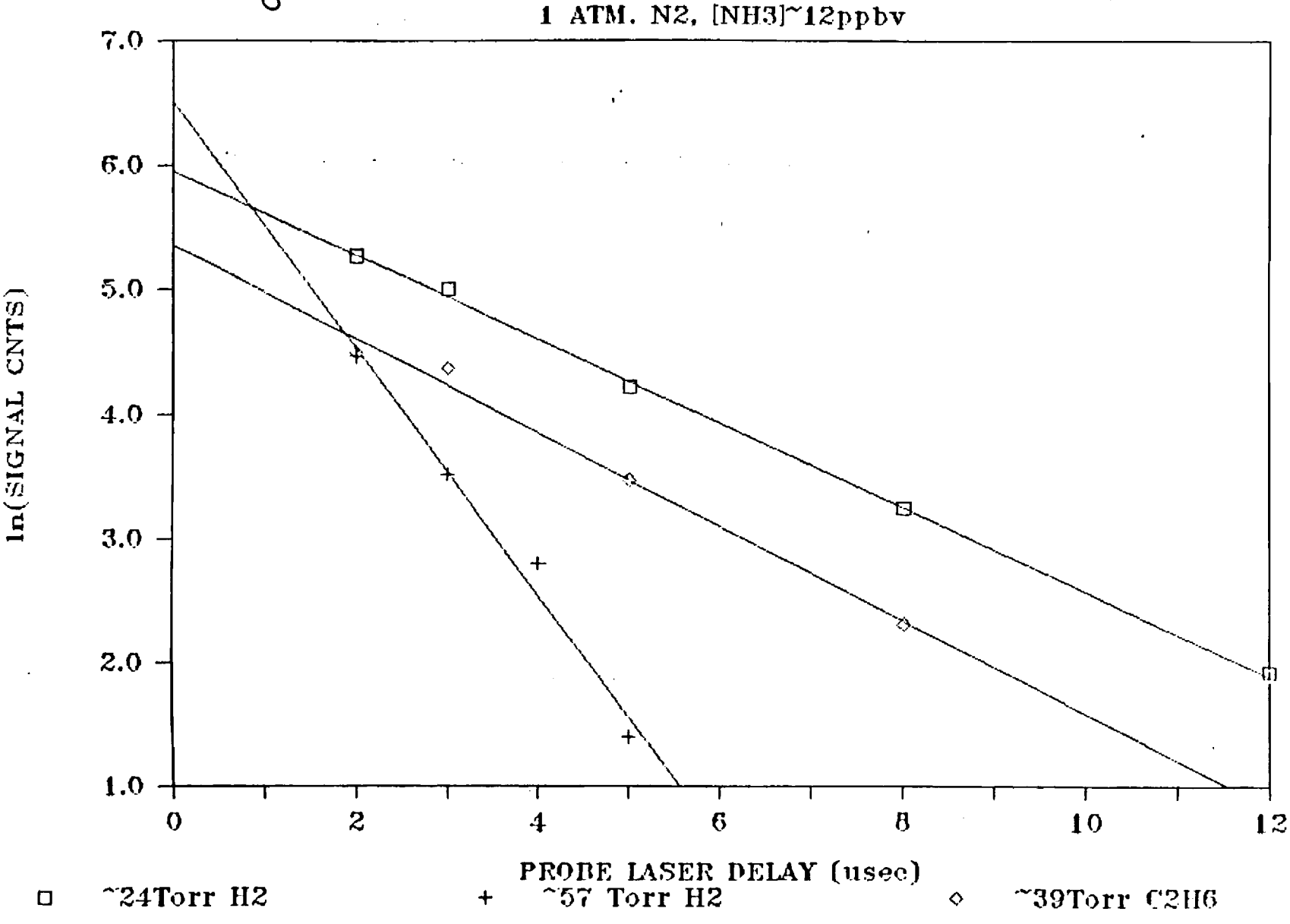

Fig. 10 [M] "QUENCHING" NH1b

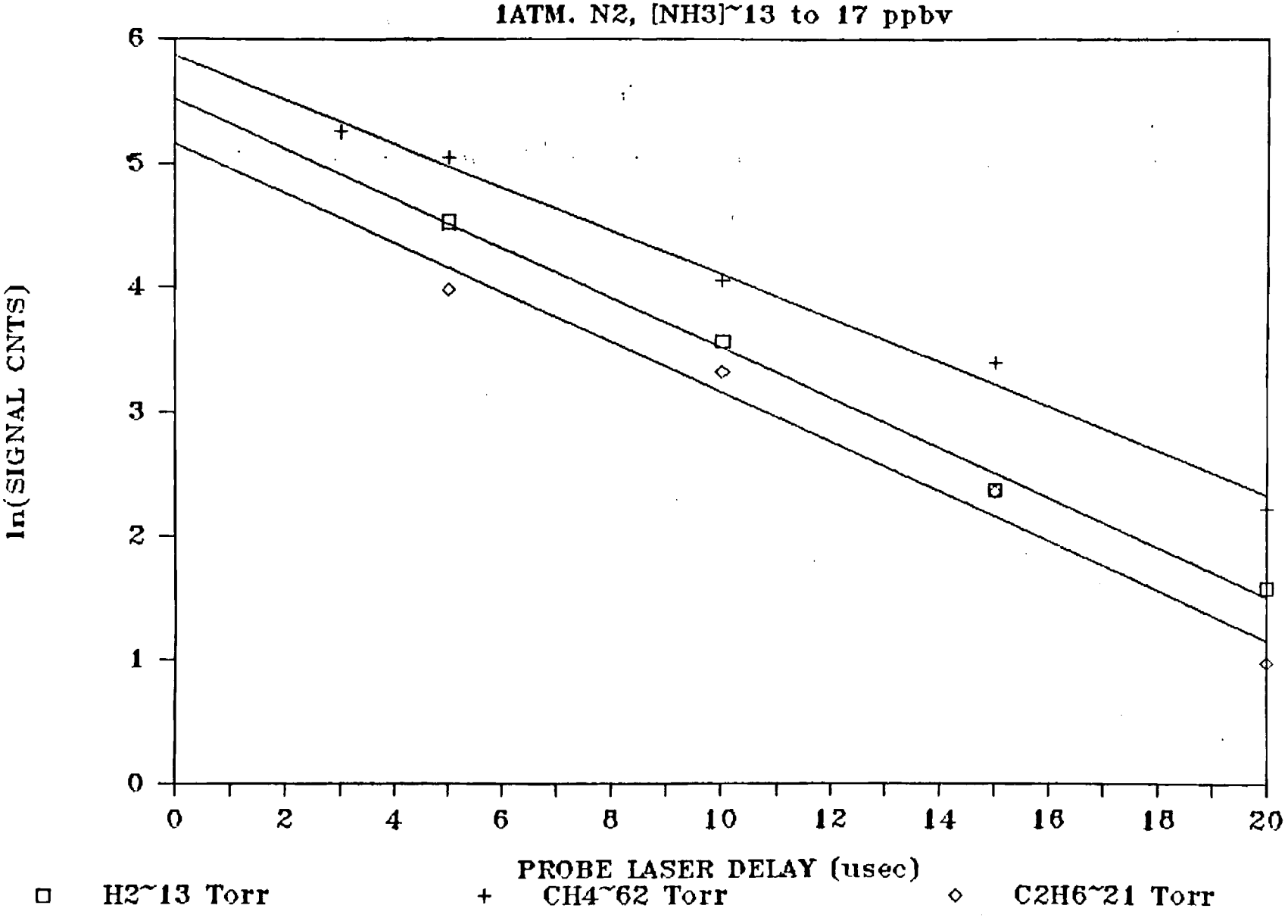

TABLE II

Rate Cooefficients for the Loss of NH'b Via Collision with the Gases H_2O, H_2, CH_4, C_2H_6, and C_3H_6

Collisional Gas Species	Concentration (Torr)	1/*e* Decay Time (μs)	k value (this work)	k value reported by Zetzsch & Stuhl (1976)
H_2O (latm N_2)*	1.97	16	9.8×10^{-13}	
H_2O (latm N_2)*	3.57	8.8	9.8×10^{-13}	
H_2O (Artif.Air)†	3.80	8.6	9.2×10^{-13}	
H_2O (Artif.Air)†	1.82	15.6	1.1×10^{-12}	
H_2O (Artif.Air)†	2.50	10.8	1.1×10^{-12}	
H_2O (Outside Air)†	6.10	5.52	8.9×10^{-13}	
H_2O (Outside Air)†	11.9	2.46	1.02×10^{-12}	
H_2O (Outside Air)†	7.9	3.56	1.06×10^{-12}	
		Ave.	$1.0\pm 08\times10^{-12}$	4.9×10^{-13}
H_2 (latm N_2)*	24.3	3.1	4.1×10^{-13}	
H_2 (latm N_2)*	57.0	1.0	5.2×10^{-13}	
H_2 (latm N_2)*	12.1	5.8	4.3×10^{-13}	
		Ave.	4.5×10^{-13}	8.6×10^{-13}
CH_4 (latm N_2)*	47.1	7.2	8.8×10^{-14}	
	62.3	6.2	7.8×10^{-14}	
		Ave.	8.3×10^{-14}	1.8×10^{-13}
C_2H_6 (latm N_2)*	22.0	5.9	2.3×10^{-13}	
	38.7	2.8	2.8×10^{-13}	
	20.5	5.4	2.7×10^{-13}	
		Ave.	2.6×10^{-13}	
C_3H_6 (latm N_2)*	.615	25	1.9×10^{-12}	4.7×10^{-13}

† Conditions: latm. of Air: 8 to 7 ppbv NH_3
* Conditions: latm. of N_2: 8 to 17 ppbv NH_3

D. FIELD MEASUREMENTS

The NH_3 field measurements reported here are those recorded on the Georgia Tech campus over the time period of May 4 to May 20, 1986. The location of the inlet system for these measurements was the Baker Building which is situated on the north central part of the Tech campus. The back side of the building, the side of the building through which we placed a 28' long, 1 1/4" I.D. pyrex sampling line, is adjacent to a lightly traveled campus road, State Street. The sampling line itself extended - 15' beyond the building wall and was - 20' above ground level. Both of the latter geometric considerations were designed to minimize the influence of the building and the ground as possible loss mechanisms for NH_3.

At the present time it is difficult to pin point all the possible sources of NH_3 on the campus or even in the immediate vicinity of the Baker Building. Certainly sewage vent pipes on the top of the Baker Building (- 50' away and centered in the middle of the roof) as well as chemical fume hood exhausts (- 70' away on the far corner of the roof) represent what we now believe are the most immediate potential sources of NH_3 relative to the location of our sample intake pipe.

Typically, a flow rate of 600ℓ/min. was maintained through the inlet line and ambient fluorescence cell, although variations in the flow rate ranging from 150ℓ/min to as high as 1200ℓ/min were used in tests to establish that the sampling line and fluorescence cell were free of any memory problems. At 600ℓ/min the residence time in the sampling network (includin the fluorescence cell) was - .6 sec.

Routine calibrations of the VUV/PF-LIF system were carried out using the standard addition technique. In our case, the primary NH_3 standard consisted of a certified bottle of 100 ppmv of NH_3 in N_2 which was obtained from Scott

Environmental Labs. The primary standard was coupled to either a two or three stage dynamic dilution system as described earlier in the text. The injection of the calibration gas occurred 4" from the inlet of our ambient air sampling line. Injection of cal-gas into the sampling line was achieved by means of a solenoid activated valve that was positioned within a few inches of the point of injection of the cal-gas into the ambient sampling line.

As can be seen from Table III, in addition to NH_3 measurements, several ancillary measurements were made during several of the longer NH_3 sampling runs. These included: WD, WS, RH, DP, visible and UV flux, O_3, NO_x, SO_2, HNO_3, aerosol composition, and rain analysis.

At this time, a detailed analysis of the urban Atlanta NH_3 data set and the data from related chemical species has not been completed. However, from Table III, some trends seem noteworthy even at this early stage in the data analysis. Over an - two week period the range of NH_3 levels was found to be .7 to 5.8 ppbv. However, in a run on 5/20/87, too new to have been incorporated into Table III, two separate NH_3 spikes occurred during the day one of which exceeded 50 ppbv. Immediate observations made outside the building during this time period showed no unusual activity, and we can only surmise that there may have been a large release of NH_3 from one of the Baker Buildings' fumehoods. There also appear to be no clear trends in the NH_3 levels for day versus nighttime sampling nor are any clear cut trends observed in the NH_3 level and Rel. Humid. or dew-point. Perhaps the most significant correlations, if any are to be found, will be those between NH_3 and HNO_3 and gas phase NH_3 levels versus NH_4^+ aerosol phase. As noted earlier these data are not yet available.

As one of several tests that were performed to determine if there were memory problems in the pyrex sampling line, we varied the flow-rate in the ambient sampling line over the range of 150ℓ/min up to 1200ℓ/min, an 8 fold change. Within the photon statistics of these measurements as well as any natural variability in the outside NH_3 level, no significant change was observed in the NH_3 signal level. Thus, we believe that the NH_3 values reported here are representative of the levels of NH_3 that were present in ambient air during the time period of 5/4/87 to 5/20/87, not artifacts of wall memory effects.

In Figs. 11, 12, 13 and 14 are shown representative real time profiles of NH_3 on days 5/5, 5/12, and 5/20. Also shown for 5/12 are the ancillary measurements, taken at the same time that NH_3 was being sampled. (The NH_3 data were recorded with 1 min. time resolution.) The gaps in some of these data (e.g. that on 5/12) represent time periods during which time tests were being performed or in somecases times during which the excimer laser was being refilled with ArF gas.

As noted earlier, there are, on the average, very few major changes that were observed in the level of NH_3 over a several hour period. The most dramatic effect observed is that shown in Fig. 14, where two NH_3 spikes occurred, separated by ~ 1 hr. in time. The first of these went from a base line level of ~ 3 ppbv to over 50 ppbv in a matter of 3 or 4 minutes and dropped back down to the base line level of 3 ppbv in approximately the same amount of time. No explanation has yet been found for this observation. There is currently no basis for believing it was an instrumental artifact.

Fig. 11 AMBIENT AIR 5/5/87

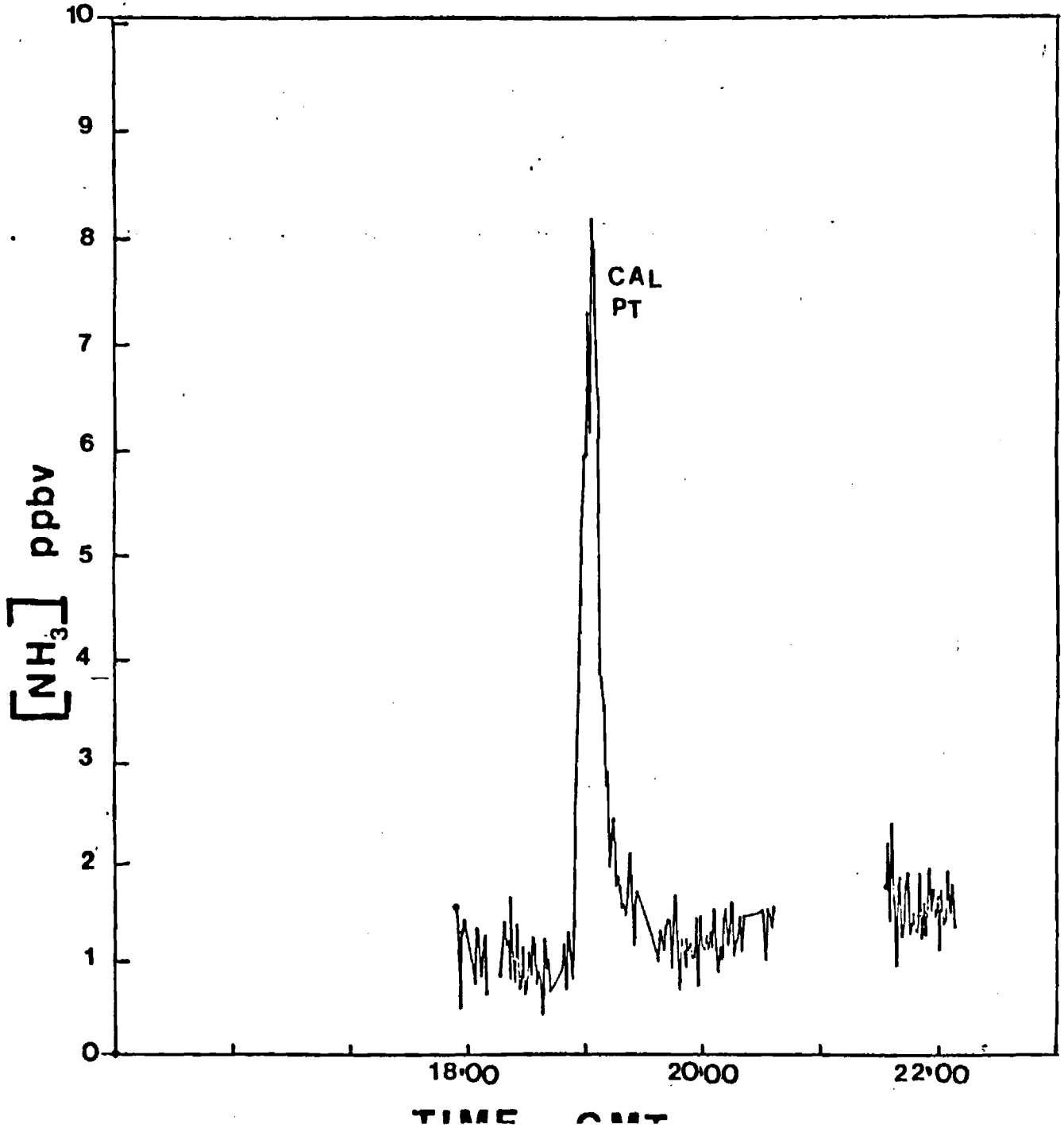

Fig 12 AMBIENT AIR 5/12/87

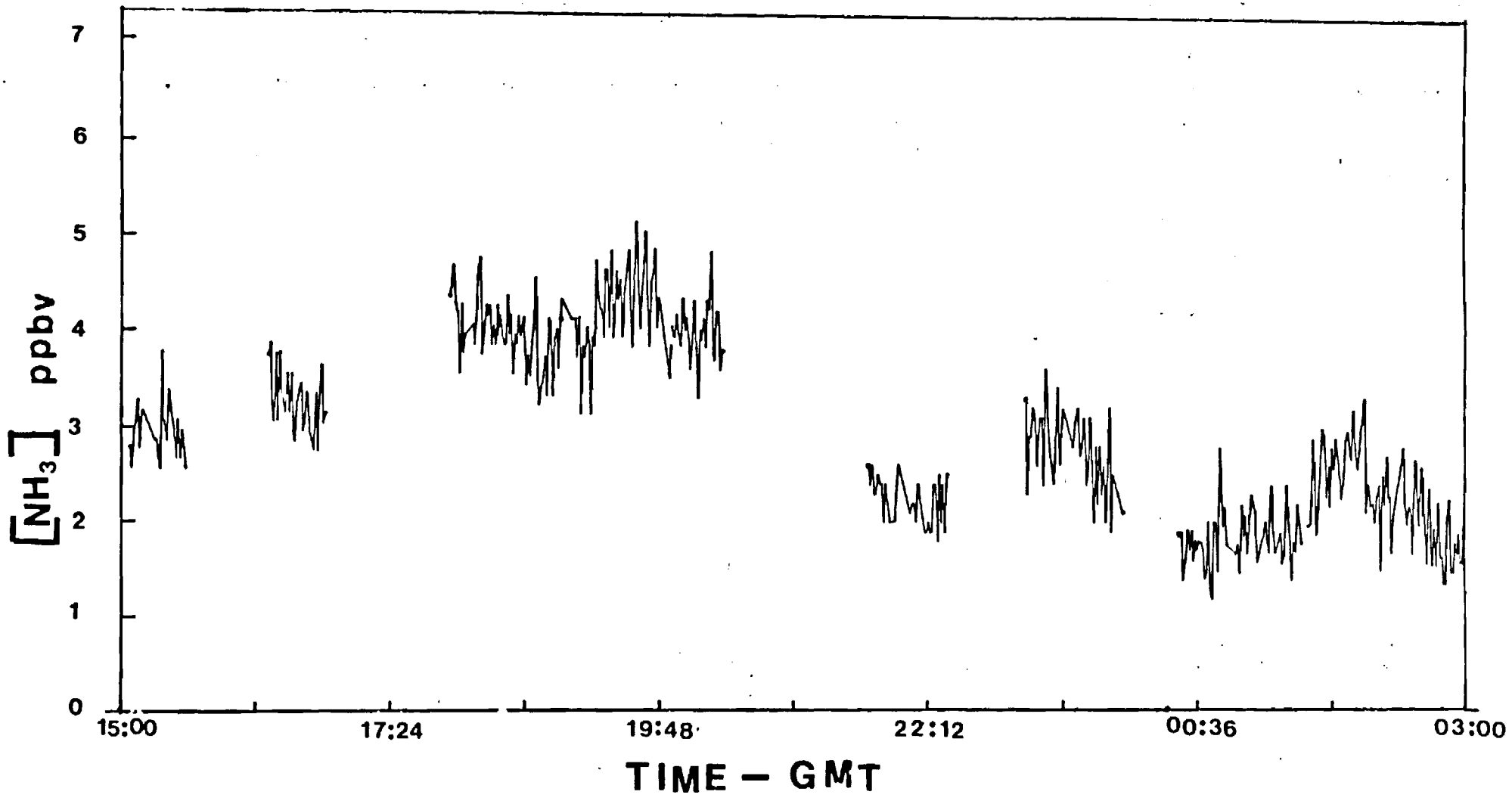

Fig. 13 05/12/87

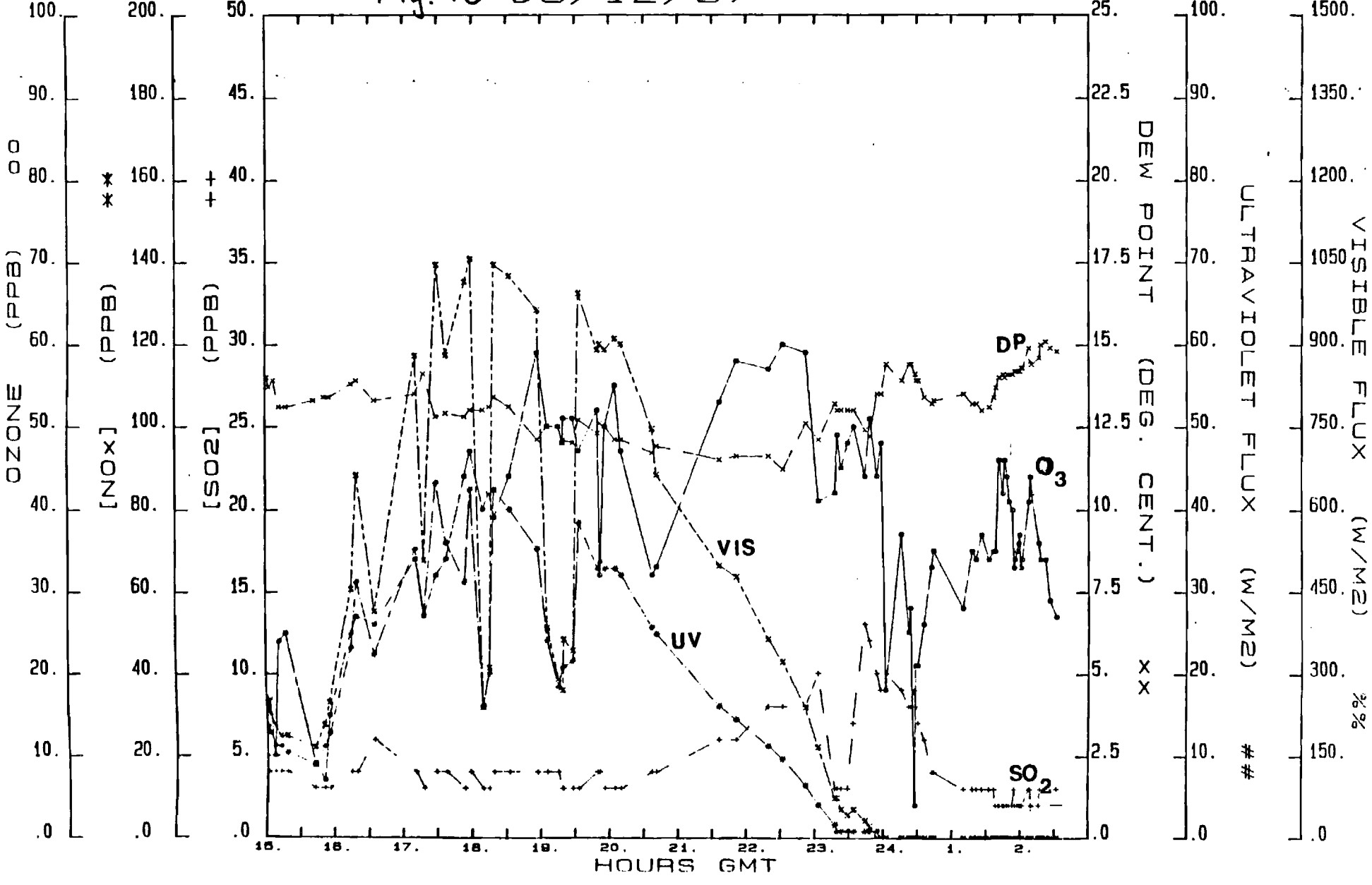

Fig 14 AMBIENT AIR 5/20/87

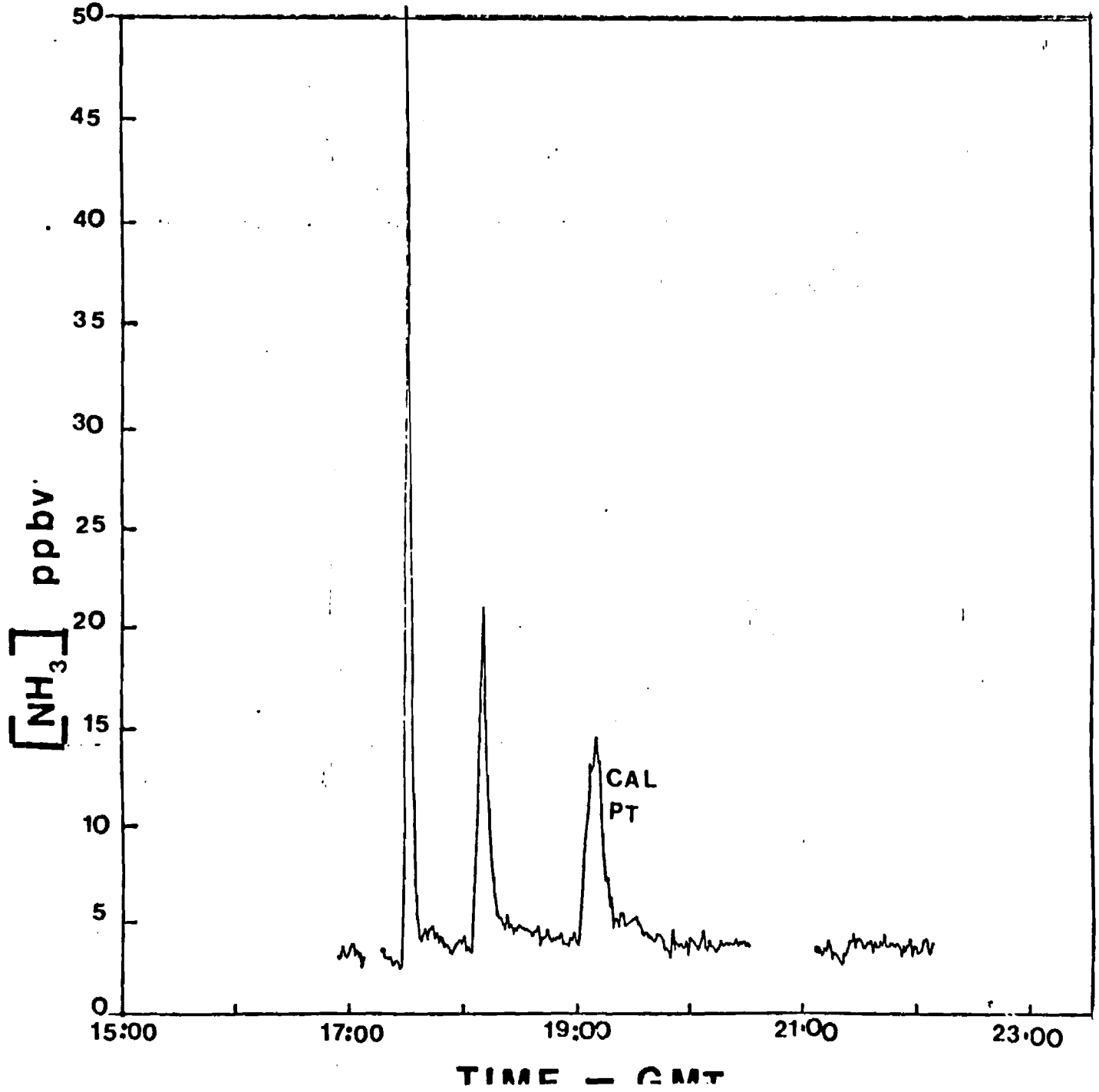

Table III Summary of NH_3 and Ancillary Measurements
on the Georgia Tech Campus Over the Time Period of May 4 → May 14, 1987

DATE	WD	WS mph	RH	DP	$[O_3]$ ppbv	$[NO_x]$ ppbv	$[SO_2]$ ppbv	$[NH_3]$	COMMENTS
05/04/87 00:00 to 02:32 GMT	NW	5	84%	+14°C	NR	NR	NR	m 1.0 (±0.2)* ℓ 0.7 h 1.7	Rain Shower Afternoon
05/05/87 12:16 to 22:10 GMT	NE	10-15	83%	+7.6°C	m=3 ℓ 0 h 7	NR	m 1.5 ℓ 1 h 2	m 1.5 (±0.25)* ℓ 0.7 h 1.7	Clear no rain
05/06/87 17:25 to 23:16 GMT	SE	10	90%	+9.4°C	m 33 ℓ 26 h 48	NR	m 16 ℓ 4 h 27	m 2.6 (±0.4)* ℓ 1.5 h 3.4	Clear no rain
05/07/87 15:30 to 22:06 GMT	NW	3-15	54%	+11°C	m 36 ℓ 20 h 54	NR	m 21 ℓ 8 h 46	m 3.3 (±0.5)* ℓ 1.8 h 4.8	Clear no rain
05/08/87 15:01 to 22:40 GMT	NE	10-16	26%	+2°C	m 68 ℓ 63 h 93	NR	m 7 ℓ 4 h 7	m 2.8 (±0.4)* ℓ 1.6 h 4.0	Clear no rain Two HNO_3 Samples
05/11/87 18:14 to 21:07 GMT	E	5-13	96%	+13.5°C	m 17 ℓ 3 h 28	NR	m 3.5 ℓ 2 h 6	m 3.4 (±0.5)* ℓ 2.2 h 4.9	Light Rain during most of time Two HNO_3 Samples

05/12/87	SE		47%	+12	m 30	m 30	m 3.5	m 2.8	(±0.3 to)*	Mostly sunny to 23:00 GMT
15:03 to	to	5-13	to	to	ℓ 1	ℓ 14	ℓ 2	ℓ 1.3		Then rain showers
04:00 GMT	NE		90%	+15	h 58	h 46	h 6	h 4.8		Three HNO_3 Samples
05/13/87	NE		58%	+14°C	m 33	m 20	Avm. 2.7	m 2.0	(±0.34)*	Partly sunny or no rain to
17:00 to	to	5-10	to	to	ℓ 14	ℓ 10	low 2	ℓ 1.2		24:00 GMT then rain at ϕ1:00
03:30 GMT	SE		93%	+15°C	h 58	h 40	high 16	h 3.0		GMT 5/14/87
5/14										Three HNO_3 samples
Diurnal										
05/14/87	E		56%	+13	m 18	m 25	Avm. 1.4	m 3.5	(±0.5)*	Cloudy most all of time,
to 05/15/87	to	6-13	to	to	ℓ 6	ℓ 8	low 1	ℓ 1.5		Light Showers
16:53 GMT	NE		100%	+15	h 42	h 95	high 2	h 5.8		Four HNO_3 samples
to 22:02 GMT										

NR = nor recorded; m = mean valve; ℓ = minimum level; h = maximum value

* Uncertainty specified is the 1σ uncertainty derived from photon statistics for a 1 min. integration time

IONAL SCIENCE FOUNDATION
Washington, D.C. 20550

FINAL PROJECT REPORT
NSF FORM 98A

PLEASE READ INSTRUCTIONS ON REVERSE BEFORE COMPLETING

PART I—PROJECT IDENTIFICATION INFORMATION

titution and Address	2. NSF Program	3. NSF Award Number
Georgia Institute of Technology Earth and Atmospheric Sciences 221 Bobby Dodd Way, Atlanta, Ga 30332	Atmospheric Sciences Div.	ATM 8610236
	4. Award Period From 6/15/86 To 2/28/89	5. Cumulative Award Amount $301,831

oject Title
Vacuum-Ultraviolet Photofragmentation/Laser-Induced Fluorescence Sensor For Measurements of Atmospheric Trace Gases

PART II—SUMMARY OF COMPLETED PROJECT *(FOR PUBLIC USE)*

The major objectives of this project were: (1) to develop a highly sensitive and selective method for detecting NH_3 adaptable to atmospheric field sampling and (2) to demonstrate the general applicability of vacuum-UV photofragmentation, in combination with laser-induced fluorescence, as a technique for detecting non-fluorescing atmospheric trace gases.

The approach used in this study involved the two photon photofragmentation of NH_3 using 193 nm radiation from an Ar excimer laser ($NH_3 + h(\lambda=193\ nm) \rightarrow NH_2 \dashrightarrow NH(b^1\Sigma^+)$), followed by the excitation at 450 nm of meta stable $NH(b^1\Sigma^+)$, i.e. $NH(b'\Sigma^+) + h_2 \rightarrow NH(c'\pi)$. Fluorescence from the $NH(c'\pi)$ species was then detected at 450 nm, e.g. $NH(c'\pi) \rightarrow NH(a'\Delta) + h_3$.

This system has been demonstrated to be a highly specific and sensitive method for the quantitative measurement of atmospheric ammonia in both independent field studies by the Georgia Tech group as well as by our participation in a large scale NSF/NCAR organized NH_3 instrument intercomparison. Limits of detection for the current instrument are 10 pptv and 4 pptv for 1 and 5 min. integration periods, respectively, for ambient sampling conditions. The technique is free from interferences and system performance does not significantly degrade in adverse sampling conditions (i.e. rain, fog, clouds, haze, etc.) Spectroscopic selectivity in the $^{15}NH(b'\Sigma^+) \rightarrow {}^{15}NH(c'\pi)$ transition is sufficient to resolve $^{15}NH_3$ and $^{14}NH_3$ contributions for use in atmospheric tracer studies and for real-time calibrations of the VUV-photofragmentation LIF ammonia system.

PART III—TECHNICAL INFORMATION *(FOR PROGRAM MANAGEMENT USES)*

TEM *(Check appropriate blocks)*	NONE	ATTACHED	PREVIOUSLY FURNISHED	TO BE FURNISHED SEPARATELY TO PROGRAM	
				Check (✓)	Approx. Date
s of Theses	✓				
on Citations		✓			
cientific Collaborators			✓		
n on Inventions		✓			
Description of Project and Results		✓			
ify)					

tigator/Project Director Name *(Typed)*	3. Principal Investigator/Project Director Signature	4. Date
		June 4, 1991

ersedes All Previous Editions

Form Approved OMB No.

PART IV - SUMMARY DATA ON PROJECT PERSONNEL

NSF Division Atm. Sciences

The data requested below will be used to develop a statistical profile on the personnel supported through NSF grants. The information on this part is solicited under the authority of the National Science Foundation Act of 1950, as amended. All information provided will be treated as confidential and will be safeguarded in accordance with the provisions of the Privacy Act of 1974. NSF requires that a single copy of this part be submitted with each Final Project Report (NSF Form 98A); however, submission of the requested information is not mandatory and is not a precondition of future awards. If you do not wish to submit this information, please check this box ☐

Please enter the numbers of individuals supported under this NSF grant.
Do not enter information for individuals working less than 40 hours in any calendar year.

*U.S. Citizens/ Permanent Visa	PI's/PD's		Post-doctorals		Graduate Students		Under-graduates		Precollege Teachers		Others	
	Male	Fem.	Male	Fem.	Male	Fem.	Male	Fem.	Male	Fem.	Male	Fem.
American Indian or Alaskan Native												
Asian or Pacific Islander												
Black, Not of Hispanic Origin												
Hispanic												
White, Not of Hispanic Origin	4		1		1		1					
Total U.S. Citizens	3		1		1		1					
Non U.S. Citizens	1											
Total U.S. & Non-U.S. ..	4		1		1		1					
Number of individuals who have a handicap that limits a major life activity.	0		0		0		0					

*Use the category that best describes person's ethnic/racial status. (If more than one category applies, use the one category that most closely reflects the person's recognition in the community.)

AMERICAN INDIAN OR ALASKAN NATIVE: A person having origins in any of the original peoples of North America, and who maintains cultural identification through tribal affiliation or community recognition.

ASIAN OR PACIFIC ISLANDER: A person having origins in any of the original peoples of the Far East, Southeast Asia, the Indian subcontinent, or the Pacific Islands. This area includes, for example, China, India, Japan, Korea, the Philippine Islands and Samoa.

BLACK, NOT OF HISPANIC ORIGIN: A person having origins in any of the black racial groups of Africa.

HISPANIC: A person of Mexican, Puerto Rican, Cuban, Central or South American or other Spanish culture or origin, regardless of race.

WHITE, NOT OF HISPANIC ORIGIN: A person having origins in any of the original peoples of Europe, North Africa or the Middle East.

THIS PART WILL BE PHYSICALLY SEPARATED FROM THE FINAL PROJECT REPORT AND USED AS A COMPUTER SOURCE DOCUMENT. DO NOT DUPLICATE IT ON THE REVERSE OF ANY OTHER PART OF THE FINAL REPORT.

Technical Description of Project and Results

The major instrumental, laboratory, and field results derived from this highly successful project have been summarized in the following two publications:

(1) NH (b'Σ+) Deactivation/Reaction Rate Constants for the Collisional Gases H_2, CH_4, C_2H_6, Ar, N_2, O_2, H_2O, and CO_2; C.A. van Dijk, S.T. Sandholm, D.D. Davis, and J.D. Bradshaw, J. Phys. Chem., 93, p. 6363, 1989.

(2) Atmospheric Ammonia Measurement Using a VUV/Photofragmentation Laser Induced Fluorescence Technique; J.S. Schendel, R.E. Stickel, C.A. van Dijk, S.T. Sandholm, D.D. Davis and J.D. Bradshaw, Applied Optics, 29, p. 4924, 1990.

Still other major results directly related (i.e. derived from) this project but funded under another NSF grant are those involving the NSF/NCAR/NOAA sponsored NH_3 instrument intercomparison study in Boulder, Colorado, Feb/Mar 1989. Five different techniques, including the VUV/PF-LIF system, were compared under both ambient as well as controlled spiked sampling conditions using a common manifold. The VUV/PF-LIF clearly demonstrates superior performance to the other techniques during this intercomparison. These results were reported on at the Spring 1991 AGU meeting. These intercomparison results will appear very shortly in an AGU publication.

Inventions/Patents

There were no inventions or patents developed/applied for during this project. All innovative ideas and technological break throughs achieved during the project have been reported on at conferences and/or provided to the public through publications, i.e.

(1) NH(b'Σ+) Deactivation/Rate Constants for the Collisional Gases H_2, CH_4, C_2H_6, Ar, N_2, O_2, H_2O, and CO_2
J. of Physical Chemistry, 93, p. 6363, 1989.

(2) Atmospheric Ammonia Measurement Using a VUV/Photofragmentation Laser Induced Fluorescence Technique,
Applied Optics, 29, p. 4924, 1990.

a reprint from Applied Optics

Atmospheric ammonia measurement using a VUV/photofragmentation laser-induced fluorescence technique

John S. Schendel, Robert E. Stickel, Cornelis A. van Dijk, Scott T. Sandholm, Douglas D. Davis, and John D. Bradshaw

Vacuum ultraviolet/photofragmentation laser-induced fluorescence has been demonstrated to be a highly specific and sensitive method for the quantitative measurement of atmospheric ammonia (NH_3). The fluorescence detected in this approach results from the two 193-nm photon photofragmentation step $NH_3 \rightarrow NH_2 \rightarrow NH(b^1\Sigma^+)$ followed by the excitation of the $NH(b^1\Sigma^+) \rightarrow NH(c^1\Pi)$ transition via a 450-nm photon with final emission being observed from the $NH(c^1\Pi) \rightarrow NH(a^1\Delta)$ transition at 325 nm. Limits of detection for the instrument presented here are <10 pptv and <4 pptv for 1- and 5-min integration periods, respectively, in ambient sampling conditions. The technique is free from interferences and system performance does not significantly degrade in adverse sampling conditions (i.e., rain, fog, clouds, haze, etc.). Spectroscopic selectivity in the $NH(b^1\Sigma^+) \rightarrow NH(c^1\Pi)$ transition is sufficient to resolve $^{15}NH_3$ and $^{14}NH_3$ contributions for use in atmospheric tracer studies. Average ammonia measurements at Stone Mountain, GA, ranged from ≃110 pptv for air temperatures <5°C to ≃240 pptv for air temperatures ≥5°C over the period from Dec. 1987 to the end of Apr. 1988. *Key words:* Ammonia detection, photofragmentation, laser-induced fluorescence.

I. Introduction

Ammonia is the dominant basic species in the troposphere and therefore significantly impacts on the acid-base chemistry of the lower atmosphere.[1-7] Gas phase ammonia, representing the most abundant reduced form of atmospheric nitrogen, is surprisingly stable in an oxidative atmosphere, exhibiting a long lifetime with respect to oxidative attack (~45 days). Ammonia's fate in the atmosphere is primarily controlled through its equilibrium with aerosol acidic compounds [namely, NH_4NO_3, $(NH_4)_2SO_4$, etc.] and aqueous droplets [e.g., $NH_3(g) \leftrightarrow NH_3(aq) \leftrightarrow (+NO_3^-)(aq) + NH_4^+ \leftrightarrow NH_4NO_3$], with eventual gas phase removal occurring through dry deposition and rainout/washout events. The equilibria of gas phase ammonia with aerosols and droplets is still not completely understood, especially at low concentrations and low temperatures in atmospheric conditions.[8-15] Sources of atmospheric ammonia are believed to be dominated by soil emission and varies significantly from region to region depending on land use practices, soil type, temperature, moisture content, and degree of animal husbandry. In addition, the role of the oceans with regard to being a net source or sink of atmospheric NH_3 is still unclear.[1,6,7,16,17]

Gas phase ammonia studies over continental regions (primarily in the northern hemisphere) show the range of ammonia concentrations generally varying between 1 and 20 parts-per-billion-by-volume (ppbv). There are few measurements of ammonia in remote regions and still fewer measurements of the vertical distribution of ammonia in the troposphere. Current estimates of the global ammonia budget have assumed globally averaged concentrations for remote regions ranging from 0.5 ppbv to 3 ppbv.[6,7,16] Measurements over the ocean, which are not significantly impacted by direct continental air masses, suggest this latter value is <0.2 ppbv.[1,17,18]

The cycling of gas phase ammonia and its effects on acid deposition, enhanced aqueous phase SO_2 oxidation, aerosol formation, production of nitric oxide in the remote atmosphere, and redistribution of nutrient nitrogen in biospheric systems has been pointed out in numerous reviews.[1,5-7]

The need for further studies, especially in remote regions, is obvious. However, few methods have currently exhibited an ability to reliably measure gas

When this work was done all authors were with Georgia Institute of Technology, School of Earth & Atmospheric Sciences, Atlanta, Georgia 30332-0340; R. E. Stickel is now with Atlanta University Center, Atlanta, Georgia 30310.

Received 20 March 1990.
0003-6935/90/334924-14$02.00/0.

phase ammonia at concentration levels relevant to that anticipated in the remote troposphere (i.e., $[NH_3] <$ 200 pptv). Direct spectroscopic techniques, involving either remote infrared differential absorption lidar[19] or *in situ* tunable diode laser absorption,[20,21] currently lack adequate sensitivity to be of use at concentration levels in the few to tens of pptv range. All other techniques, reported to date, indirectly determine ammonia through the use of preconcentration with subsequent analysis using chemical converters, ion chromatography, absorption or fluorescence of NH_3 derivatives, etc.

Acid impregnated filter collection techniques have been shown to possess interferences associated with either prefilter release of ammonia from ammonia containing aerosols or ammonia loss resulting from reaction with acidic deposits, or both. They can also exhibit a decrease in ammonia collection efficiency at low ambient relative humidities.[22–26] Sample collection time necessary at low concentrations is typically 3–12 h.

Acid coated diffusion denuder collection techniques have also been developed.[23,27] This method has been shown to work best when the denuder is used without a front end inlet system[28] and is limited with regard to the sample collection time necessary at low concentrations (typically 1–10 h).

Permeable membrane scrubber collection techniques have also been described recently.[29,30] The open air collection geometry[30] appears to suffer interferences from other concomitant trace gases (e.g., NO_2 and SO_2). The annular diffusion denuder sampler[29] appears promising at high concentrations (i.e., $[NH_3]$ > 250 pptv). However, problems have been exhibited at low concentrations (i.e., nonlinear response). In addition, system response changes with relative humidity are not well understood, and the discrepancy observed between results taken with and without a prefilter might suggest that small aerosols are also being collected and measured in these systems.

Metal oxide denuder collection techniques, using either tungstic oxide coated cylindrical denuders or molybdenum oxide annular denuder designs, have also been developed.[31–33] These systems rely on high temperature desorption of the ammonia from the metal oxide surface with subsequent or simultaneous catalytic oxidation of NH_3 to form the detected species NO. Interferences from other organic amines and in some cases HNO_3 have been observed. Due to the elevated temperature used in the heated Teflon inlet system, that was found to be necessary for reducing inlet memory effects,[33] interferences are likely in this latter instrument from the decomposition of concomitant ambient aerosols. Time resolution of these systems for ambient NH_3 in the tens of pptv range is currently limited to 30 min or longer.

Atmospheric ammonia measurements reported to date have been made with one of the techniques described above or a slight variation in one of the techniques listed. In general, the databases for concentrations >1 ppbv should be reasonably reliable. However, interpretation of the reliability of measurements made significantly below 1 ppbv is difficult due to the potential positive and negative interferences, which may arise in ambient sampling conditions, that are difficult to test for in a quantitative manner. Ammonia measurements in the tens of pptv range are further complicated by the adsorption properties of NH_3 and the fact that humans emit substantial quantities of NH_3, which may effect blank measurement repeatability in techniques that require human manipulation of the sample.

Reported here is a vacuum ultraviolet photofragmentation laser-induced fluorescence (VUV/PF-LIF) sensor that is capable of routine measurements of gas phase ammonia in the concentration range relevant to the remote troposphere with time resolution capabilities of 1 min or less. The VUV/PF-LIF sensor is spectroscopically selective and virtually free from inlet memory problems due to its unique high flow rate ambient sampling design. In addition, the VUV/PF-LIF NH_3 instrument has now participated in an NH_3 instrument critical intercomparison (Boulder, CO, Jan.–Mar. 1989).[34]

II. Description of VUV/PF-LIF NH_3 Sensor

A. VUV/PF-LIF Technique

Like numerous other atmospherically important polyatomic trace gases that possess unbound upper electronic states (namely, HONO, HNO_3, H_2S, CS_2, COS, etc.), ammonia does not fluoresce strongly enough to allow a direct laser-induced fluorescence (LIF) sensor to be developed with adequate sensitivity for atmospheric monitoring purposes. The method of photofragmentation laser-induced fluorescence (PF-LIF), in which the parent molecule is photolyzed into smaller fragments that possess high fluorescence efficiency, has now been demonstrated as a selective and sensitive technique for detecting the molecules HONO[35] and NO_2.[36]

The extension of the photofragmentation process into the near VUV makes possible the potential detection of numerous atmospherically important trace gases (namely, NH_3, H_2S, SO_2, CS_2, etc.). This is a result of the large absorption cross section of these gases in the VUV and the usually large quantum yields for production of simple diatomic photofragments (e.g., NH, SH, SO, CS). To assess the attributes of the VUV/PF-LIF technique, we chose ammonia as the first molecule for which to develop and test a field sensor.

The spectroscopy of the NH_3 VUV-PF/LIF detection scheme is summarized below and in the energy level diagram depicted in Fig. 1:

$$NH_3 + 2h\nu_1 \xrightarrow{\lambda_1 = 193\ \text{nm}} NH(b^1\Sigma^+) + \text{products}, \quad (1)$$

$$NH(b^1\Sigma^+, v'' = 0) + h\nu_2 \xrightarrow{\lambda_2 = 452\ \text{nm}} NH(c^1\Pi, v' = 0), \quad (2)$$

$$NH(c^1\Pi, v' = 0) \xrightarrow{\lambda_3 = 325\ \text{nm}} NH(a^1\Delta, v'' = 0) + h\nu_3. \quad (3)$$

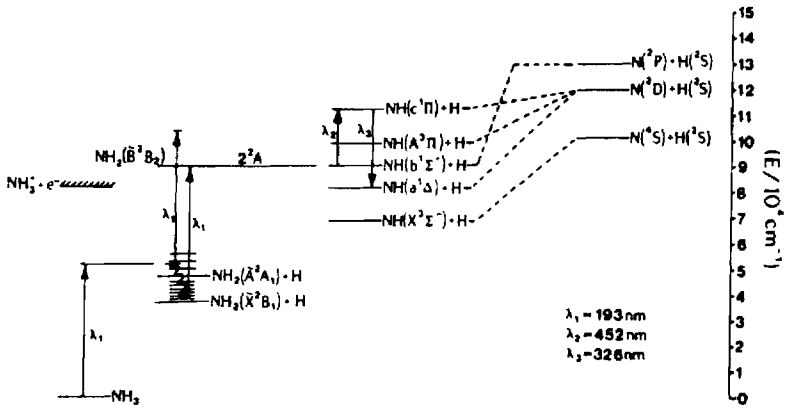

Fig. 1. Energy level diagram illustrating the VUV photofragmentation and laser-induced fluorescence steps.

Although prompt luminescence, following the photodissociation of NH_3, has been observed from several excited states of the NH photofragment, the utilization of this luminescence for development of a sensitive and selective atmospheric sensor (as suggested by Halpern *et al.*[37]) is severely complicated by the large background fluorescence (also referred to as air glow) generated from concomitant gases and aerosols by the 193-nm VUV photolysis pulse. For this reason we chose to monitor the population formed photolytically in the metastable $NH(b^1\Sigma^+)$ state. In atmospheric pressure/composition conditions, the excited $NH(b^1\Sigma^+)$ state has been found to exhibit a long enough lifetime to allow virtually all the 193-nm generated background noise to decay to near negligible levels. Thus, after an appropriate delay time (1–10 μs), the $NH(b^1\Sigma^+)$ state population can be interrogated via step (2) using a probe laser (λ_2 = 452 nm) that is capable of resolving individual rovibronic transitions in the $NH(b^1\Sigma^+) \rightarrow NH(c^1\Pi)$ manifold (Fig. 2). The fluorescence induced by the excitation to the $NH(c^1\Pi)$ state is then monitored at 325 nm. In this scheme, the observed fluorescence is spectrally blue shifted from the probe laser wavelength. This combination allows the NH_3 VUV-PF/LIF sensor to spectrally eliminate background generated from the probe laser, and temporally minimize the photolysis laser generated background to nearly insignificant levels.

The detailed nature of the two-photon process that leads to the formation of the $NH(b^1\Sigma^+)$ state is still not fully understood but is believed to involve initial formation of the $NH_2(\tilde{A}^2A_1)$ state and/or highly vibrationally excited NH_2 [e.g., reactions (4),(5) and/or (6),(7)] as shown below:

$$NH_3 + h\nu_1 \xrightarrow{\lambda_1 = 193\ \text{nm}} NH_2(\tilde{A}^2A_1) + H, \quad (4)$$

$$NH_2(\tilde{A}^2A_1) + h\nu_1 \xrightarrow{\lambda_1 = 193\ \text{nm}} NH(b^1\Sigma^+) + H, \quad (5)$$

$$NH_3 + h\nu_1 \xrightarrow{\lambda_1 = 193\ \text{nm}} NH_2^{**} + H, \quad (6)$$

$$NH_2^{**} + h\nu_1 \xrightarrow{\lambda_1 = 193\ \text{nm}} NH(b^1\Sigma^+) + H. \quad (7)$$

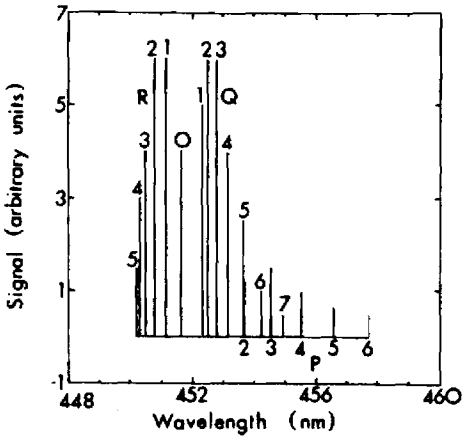

Fig. 2. Plot of relative fluorescence signals vs excitation wavelength observed for several rotational lines of the *P*, *Q*, and *R* branches of the $NH(c^1\Pi, v' = 0 \rightarrow b^1\Sigma^+, v'' = 0)$ transition.

Even though transient intermediate states are involved in this two-photon process, the overall photofragmentation process occurs with high efficiency within the short (8-ns) time period of the 193-nm photolysis laser pulse. More detailed discussions of this process are available in the literature.[38–42]

Following the formalism used previously for describing similar LIF and PF-LIF techniques,[43–45] the detection efficiency of the VUV/PF-LIF sensor can be described by

$$D_{\lambda_3} = E_{p_1} \times E_{\lambda_2} \times E_b \times E_f \times E_d \times V \times [NH_3], \quad (8)$$

where D_{λ_3} represents the number of detected signal photons per laser pulse per molecule of NH_3. The terms in Eq. (8) can further be defined as follows:

E_{p_1} = photolysis efficiency at λ_1 for producing $NH(b^1\Sigma^+)$

$$= [1 - \exp[(-p_{\lambda_1}\sigma_{\lambda_1})/a_{\lambda_1}]] \times [1 - \exp[(-p_{\lambda_1}\sigma'_{\lambda_1})/a_{\lambda_1}]] \times R, \quad (9)$$

E_{λ_2} = optical pumping efficiency at λ_2

$$= [1 - \exp(-P_{\lambda_2}\sigma_{\lambda_2})/a_{\lambda_2}] \times f_i, \quad (10)$$

E_b = efficiency of preserving $NH(b^1\Sigma^+)$ population

$$= \exp(-t_d k_{qb}[M]), \quad (11)$$

$$E_f = \text{fluorescence efficiency} = k_f/(k_f + k_{qc}[M]), \quad (12)$$

$$E_d = \text{optical detection efficiency} = \gamma_{\lambda_3} \times Y_{\lambda_3} \times Z_{\lambda_3} \times \phi_{\lambda_3}, \quad (13)$$

$$V = \text{volume of the sampling region} = a_{\lambda_1} \times l \text{ for } a_1 < a_2. \quad (14)$$

In these equations, $[NH_3]$ is the concentration of ammonia in molecules/cm^3; P_{λ_1}, P_{λ_2} represent the laser photons per laser pulse at λ_1 or λ_2; σ_{λ_1}, σ'_{λ_1}, and σ_{λ_2} represent the absorption cross section for NH_3, the intermediate NH_2, and the $NH(b^1\Sigma^+)$ transition of interest, respectively; a_{λ_1} and a_{λ_2} are the beam areas defined by the λ_1 and λ_2 lasers; f_i is the fractional population of $NH(b^1\Sigma^+)$ in the quantum state that can be pumped at 452 nm; R is the fraction of NH_3 that has undergone step (4) or (6) and that is available to participate in step (5) or (7); t_d is the time delay between photolysis and the probe laser; k_{qb} and k_{qc} are the bimolecular quenching rate coefficients for the $NH(b^1\Sigma^+)$ and $NH(c^1\Pi)$ states, respectively; $[M]$ is the concentration of quenching species; and k_f is the rate of spontaneous emission. Equations (13) and (14) define the overall efficiency at which fluorescence is detected, where γ_{λ_3} is the fraction of the total fluorescence falling within the optical transmission window; Y_{λ_3} is the total optical collection efficiency $f/1.4$ lens system; Z_{λ_3} is the optical filter transmission factor; ϕ_{λ_3} is the quantum efficiency of the photomultiplier tube (PMT) at λ_3; a_{λ_1} is again the effective beam area; and l is the effective path length over which fluorescence can be monitored by a single PMT using $f/1.4$ lenses.

Equations (8)–(14) are useful in estimating order of magnitude detection efficiencies of a VUV/PF-LIF NH_3 sensor. However, more quantitative estimates of D_{λ_3} are limited by the large uncertainties in the photofragmentation process that forms the $NH(b^1\Sigma^+)$ state. Nevertheless, these efficiency terms are useful in describing the various parameters that control the detection and operational characteristics of the VUV/PF-LIF sensor.

Equation (9), which describes the photolytic efficiency for production of $NH(b^1\Sigma^+)$ from NH_3, can be further simplified, in the absence of population depletion of the states being excited, to the form

$$E_p = (P_{\lambda_1}/a_{\lambda_1})^2 \times (\sigma_{\lambda_1}\sigma'_{\lambda_1}) \times R. \quad (15)$$

Similarily, Eq. (10) can be simplified to the form

$$E_{\lambda_2} = (P_{\lambda_2}/a_{\lambda_2}) \times (\sigma_{\lambda_2} f_i). \quad (16)$$

Thus, for laser pumping conditions that do not significantly deplete the population of the state being pumped, the detection efficiency is proportional to the square power of the photolysis laser photon flux and to the first power of the probe laser photon flux as shown below:

$$D_{\lambda_3} \propto (P_{\lambda_1}/a_{\lambda_1})^2 \times (P_{\lambda_2}/a_{\lambda_2}) \times [NH_3]. \quad (17)$$

Confirmation of this relationship has demonstrated a linear regression analysis for $\log(D_{\lambda_3})$ vs log (photolysis laser pulse energy per unit area), with a slope of $1.7 \pm 0.3(2\sigma)$, over the range of 2–23 mJ/cm^2, and with no obvious signs of saturation affects. The deviation from true square power dependency (i.e., slope = 1.7) is believed to be due to the temporal waveform of the excimer laser pulse and the functionality of P_{λ_1}, P_{λ_2}, and R with time which are not accounted for in the simple assumption of square root dependency. The dependence of D_{λ_3} on the 452-nm probe laser energy fluence exhibited a log–log slope of $0.97 \pm 0.08(2\sigma)$ for laser energy fluences from 0.05 to 2.5 mJ/cm^2.

Equation (11) defines the efficiency that the $NH(b^1\Sigma^+)$ state population, formed from the photolysis of NH_3, survives the delay time between photolysis and probe laser pulses. Detailed studies into the relaxation effects of the most atmospherically important collision partners (e.g., $M = H_2O$, O_2, N_2, CO_2) have been carried out as previously reported.[46] Of these molecules, water vapor was found to be the most important component in terms of deactivating the $NH(b^1\Sigma^+)$ state with $k_{qb} = 1.0 \pm 0.07 \times 10^{-12}$ cm^3 molecule^{-1} s^{-1}. For a nominal probe laser delay time of $t_d = 2$ μs, E_b is found to vary from 0.94 to 0.37 over the range of water vapor concentration of 1–15 Torr that could be encountered over the altitude range of 10–0 km, respectively.

Tests were also carried out to determine the rotational population distribution, within the $NH(b^1\Sigma^+)$ state, that defines f_i. The distribution of population was found to be thermalized into a Boltzmann distribution [$T = 292 \pm 5$ K(2σ)], within 2 μs, by probing the Q-branch rovibronic transitions $Q1$–$Q7$ with either Ar or N_2 as the buffer gas. No pressure (i.e., altitude) dependency is anticipated in the collisional redistribution of the $NH(b^1\Sigma^+)$ state over the ambient sampling pressure range of 200–1000 mbar (i.e., 10–0km altitude) for probe laser delays of $t_d \geq 2$ μs.

The $NH(c^1\Pi)$ state fluorescence efficiency defined by Eq. (12) is controlled by the collisional quenching term $k_{qc}[M]$. The bimolecular rate constant for O_2 as a collision partner ($k_{qc} = 1.9 \pm 0.2 \times 10^{-10}$ cm^3 molecules^{-1} s^{-1})[47] is found to dominate the relaxation process for the $NH(c^1\Pi)$ state. As with other LIF techniques, the effect of pressure changes (i.e., altitude) on D_{λ_3} is negligible when the NH_3 concentration is expressed in terms of a mixing ratio (i.e., pptv) rather than as an absolute concentration (molecules/cm^3).[43,44]

The parameters effecting the optical detection efficiency E_d [Eq. (13)] and the observed fluorescence volume V [Eq. (14)] have been optimized to the extent possible where $\gamma_{\lambda_3} \simeq 0.95$, $Y_{\lambda_3} \simeq 0.01$ (over $l = 2$ cm); $Z_{\lambda_3} \simeq 0.4$; $\phi_{\lambda_3} \simeq 0.3$; $a_{\lambda_1} \simeq 0.3$ cm^2; and $l \simeq 2$ cm. As defined, D_{λ_3} is the detection efficiency in terms of observed photons per laser pulse per photomultiplier. D_{λ_3} can be increased when expressed in per unit time by integrating the observed fluorescence over multiple laser pulses (i.e., integration time × pulse rate repetition rate). D_{λ_3} can also be increased be increasing the number of photomultiplier tube/collection optics sys-

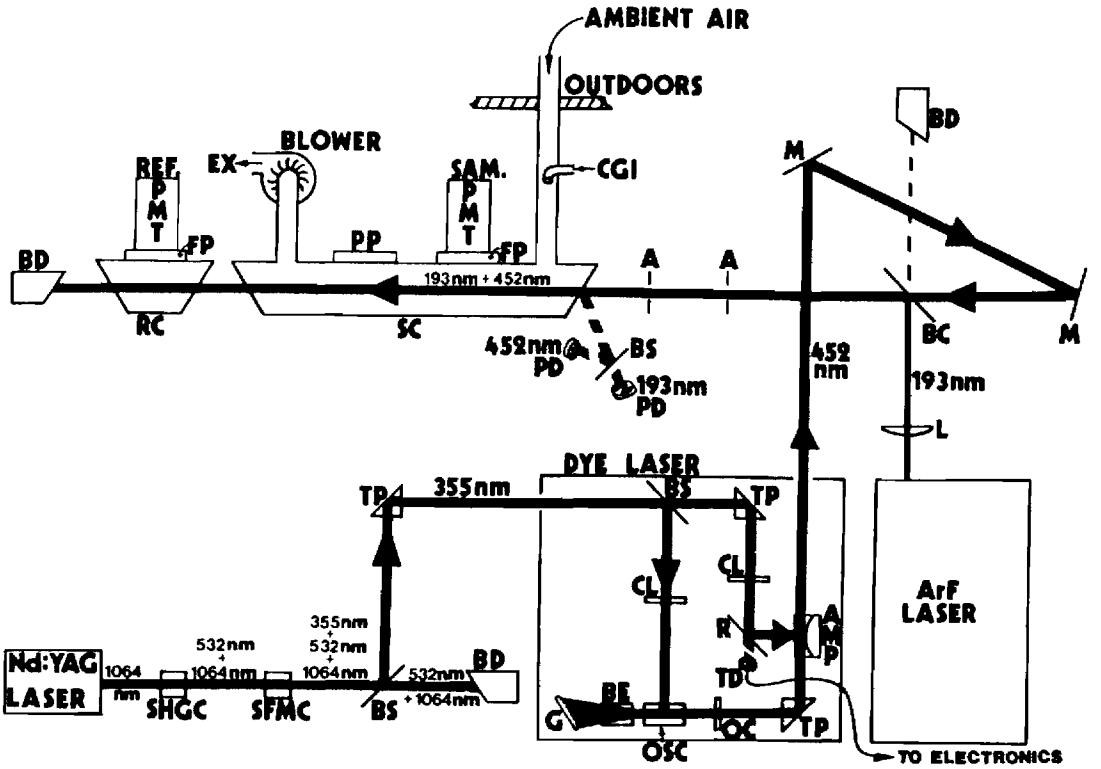

Fig. 3. Schematic representation of the NH_3 sensor: *SHGC*, second harmonic generation crystal; *SFMC*, sum frequency mixing crystal; *BS*, beam splitter; *BD*, beam dump; *TP*, turning prism; *CL*, cylindrical lens; *R*, reflector; *TD*, trigger diode used to provide the gate timing signal; *OSC*, oscillator cell; *AMP*, amplifier cell; *BE*, beam expander; *G*, grating; *OC*, output coupler; *M*, mirror; *BC*, beam combiner; *L*, lens; *A*, aperture; *PD*, photodiode used to monitor laser pulse energy; *SC*, sample cell; *RC*, reference cell; *FP*, filter pack; *SAM. PMT*, sample cell photomultiplier; *REF. PMT*, reference cell photomultiplier; *PP*, additional photomultiplier port; *EX*, exhaust; *CGI*, calibration gas inlet to flow line.

tems viewing the fluorescence zone which effectively increases the observed volume V. In general, further optimization of Y_{λ_3} is limited by the degradation in the rejection properties of the bandpass filter for off-axis (i.e., noncollimated) light.

B. Experimental Hardware

Figure 3 depicts a schematic of the experimental apparatus. The 193-nm photolysis laser was an ArF excimer laser (Quanta Ray Exc-1) that produced a nominal output energy of 14 mJ/pulse with an 8-ns temporal width, 1- × 1-cm beam area, and a 3-mrad beam divergence. To optimize the term E_{p_1} [$E_{p_1} \propto$ (193-nm laser energy per unit area)^{1,7}], the photolysis laser beam was softly focused, using a 1.5-m focal length lens, to ~0.3 cm^2 at the center of the sample cell (where the energy was ~9 mJ/pulse). The probe laser consisted of a Nd:YAG pumped dye laser (International Laser System NT674 and Quanta Ray PDL-1, respectively). The laser dyes employed were coumarin 450 for the laser oscillator and coumarin 460 for the side pumped amplifier. The dyes were pumped by the third harmonic output of the Nd:YAG laser (λ = 355 nm). Different oscillator/amplifier dyes were chosen to reduce spectrally broadband amplified spontaneous emission from the dye laser. The probe laser beam was spatially filtered and collinearly combined with the 193-nm photolysis laser and had an energy of ~2 mJ/pulse, in an 0.8-cm^2 beam, at the sample cell. Pulse energies of both laser beams were monitored by silicon photodiodes. The larger probe laser beam area, a_{λ_2}, was chosen to minimize spatial overlap problems between λ_1 and λ_2 lasers in a field instrument.

Extensive tests were carried out, early in the sensor development program, to select materials that would both minimize the 193-nm generated background signal and memory effects caused by adsorption of NH_3. The trend in the magnitude of the 193-nm generated background fluorescence for some of the materials tested was found to be vitreous carbon ≪ stainless steel (316 or 324), passivated nickel, aluminum (6061) < brass, black Teflon coated aluminum, Pyrex, anodized aluminum < crown glass, S1-UV quartz < (G1, 12-IR, or CO) grade quartz, sapphire (where each < symbol represents approximately a factor of 4 lower fluorescence). Vitreous carbon would have been the ideal choice of cell materials but was abandoned due to the complexities and costs involved in fabricating a cell from this material. Passivated nickel (a material with low NH_3 memory),[48] having lower background fluorescence than Pyrex or S1-UV quartz, was chosen for the sample cell body and S1-UV quartz for the optical window materials (due to the transmission requirements needed at 193 and 325 nm).

The fluorescence light was collected using a pair of f/1.4 S1-UV lenses in a point-collimated-point geometry and imaged onto a photomultiplier tube (PMT, Hamamatsu model R331). A Schott UG-11 and a 50-Å bandpass filter (centered at 325 nm, Barr Associates) were placed in the collimated region of the collection optics package and used to reject background light not falling within the $NH(c^1\Pi) \Rightarrow NH(a^1\Delta)$ fluorescence band profile.

The R331 PMT was operated in a virtual grounded cathode configuration, to which a +450-V gating pulse could be applied. This pulse effectively gated off the PMT during the 193-nm photolysis laser pulse. The PMT on/off contrast ratio, using this configuration, was >100/1. Gating of the PMT in this manner was necessary to reduce PMT self-generated noise caused by the large background signal that was observed during the 193-nm photolysis laser pulse. Use of a high speed gated microchannel plate PMT (Hamamatsu model 1564) having >1000/1 contrast ratio showed no statistically significant change in the observed background over that observed with the less expensive gating scheme using the R331 PMT.

Time synchronization of the gate generator and laser pulses was provided by an in-house-constructed synchronization/timing system. Delay times between the photolysis and probe laser could be varied from 2 μs to 10 ms. Photolysis to probe laser jitter was <0.2 μs. The high speed gated photon counting electronics have been described previously.[49]

Ambient sample manifolds have been constructed of 5-cm i.d. heavy wall Pyrex tubing having lengths that vary from <1.5 m (for an aircraft sampling platform) to as long as 8 m (for a ground based system). As noted in Eq. (8), the VUV/PF-LIF signal is independent of sample volume flow rate. The use of high volume sampling flows that produce short residence times has been an effective means of minimizing memory problems associated with NH_3 adsorption on the inlet sample manifold walls. Typical sample flow rates, used in this system, range from 600 to 2400 slpm with sample residence times of <1 s. The residence time within the optical cell was <0.1 s. To minimize aerosol decomposition effects, pressure drops within this nonrestricted sample manifold were kept below 5 mbar. In addition, the sample manifold and cell were thermally insulated and operated within ±3°C of ambient air temperature. The sample inlet manifold and optical cell were routinely leak tested using 100 ppmv of $^{15}NH_3$ (see discussion in next section) as a tracer gas.

Calibration of the instrument has been accomplished in a three tier manner. Data normalization, using the VUV/PF-LIF signal measured from a referencing cell that contains a known mixture of NH_3 and nitrogen, constituted the first tier. This reference cell system is instrumentally equivalent to an internal standard and was used to correct for degradations in laser performance that can occur between calibrations (namely, laser energy and wavelength drifts).[49] The signal from the reference system was continuously recorded by the data acquisition/computer system and was used to normalize all data. The second tier involved calibrations using isotopic $^{15}NH_3$ as a working gas standard. The spectroscopic selectivity of the VUV/PF-LIF approach makes possible the resolution of $^{15}NH(b^1\Sigma^+,v'' = 0) \Rightarrow {}^{15}NH(c^1\Pi,v' = 0)$ individual rotational transitions from their ^{14}NH counterparts. Contrast ratios between signals from ^{15}NH and ^{14}NH, for the strongest $Q(1)$, $Q(2)$, and $Q(3)$ lines, were typically 5:1, 18:1, and 30:1, respectively. Due to the lack of a laser line narrowing etalon in the dye laser used in these experiments, the observed contrast ratios were inadequate for the direct determination of ambient $^{15}NH_3$. Isotopic $^{15}NH_3$ has, however, been found to provide reliable standard addition calibrations at concentrations near that of ambient $^{14}NH_3$, even in conditions where the ambient ammonia concentration was highly variable. The third calibration tier involved direct calibration of the system by the method of standard addition using a primary $^{14}NH_3$ certified gas standard. The standard addition calibration system consisted of a three-stage continuous flow serial (dynamic) dilution system, which has been previously described.[49] This system diluted 100-ppmv NH_3 certified standards (Scott Specialty gases) and provided a continuous flow of nominally from 100-ppbv to 1-ppmv NH_3 to a solenoid valve mounted at the inlet of the ambient sampling manifold. Standard addition calibration, using either $^{15}NH_3$ or $^{14}NH_3$, covering the range of 0.1–10 ppbv was accommodated by varying the gas flow rate admitted to the sampling manifold from the preequilibrated calibration flow loop.

Dew point, within the sample manifold, was monitored using a two-stage dew-point hygrometer (General Eastern) and was used to correct for changes occurring in ambient water vapor between calibration points, as described earlier in Eq. (10).

Data acquisition computer systems were used to record the VUV/PF-LIF signal counts, laser energy monitor and reference signals, dew point, sample manifold and ambient temperature, calibration system and ambient flow measurements, as well as other system parameters and chemical/meteorological variables [namely, O_3 (Dasibi photometer), windspeed and direction, pressure, etc.]. These systems were nominally operated in 1–5-min data formats representing the integrated value of fluorescence signal counts or the average value of support data over these time periods.

C. Operational/Performance Characteristics

As previously mentioned, the sensitivity of the instrument (i.e., D_{λ_3}) is strongly dependent (1.7 power) on the 193-nm photolysis laser energy. This energy can vary from 18 to 4 mJ/pulse as the performance of the excimer laser slowly degrades over a period of months between routine servicing intervals. In critical applications, where utmost sensitivity is required, the laser can be maintained at high output energies for operational periods in excess of 240 h between maintenance intervals. In these conditions (nominal laser output energy = 14 mJ/pulse) the instrument sensitivity for the configuration reported here has been found

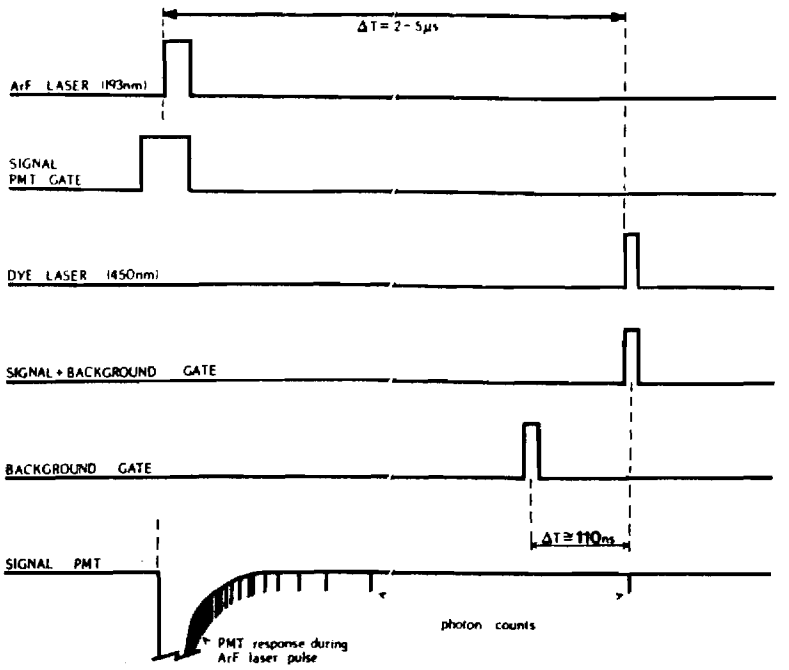

Fig. 4. Timing diagram of the NH_3 sensor. Just prior to the ArF (193-nm) laser pulse, the signal photomultiplier is gated off so that its response to white fluorescence produced by the ArF laser is minimized. From 2 to 5 μs after the ArF laser pulse and 110 ns before the 450-nm laser pulse, the background gate is opened briefly (Δt = 15 ns) to allow background photon counts to be recorded. When the dye laser pulse occurs, the signal + background gate is opened (Δt = 15 ns) such that signal + background photon counts are recorded.

to be 1.5 ± 0.3-photons/pptv/min integration (at 10-Torr water vapor concentrations and t_d = 2 μs).

The detection limit (LOD) of the sensor has been found to be limited by the photon statistical fluctuations [i.e., (background counts)$^{1/2}$] in the observed 193-nm photolysis laser generated luminescence. The absolute magnitude of the observed 193-nm generated background component, which typically ranges between 1 and 20 photons/min (at t_d = 2 μs) depending on the concomitant loading of aerosols and trace gases in the ambient air, is continuously monitored by a separate gated photon counting channel, whose aperture opens ~110 ns prior to (or after) the fluorescence induced by the probe laser pulse. The timing diagram depicting this sequence is shown in Fig. 4. For conditions of low relative humidity, longer photolysis to probe delay times can be used to further minimize the observed background, which has been found to decay with a nominal $1/e$ time of 3^{+2}_{-1} μs (over the time range of 2 μs < t_d < 20 μs). As currently configured, this system, using one fluorescence detection PMT, has exhibited LODs (S/N = 2/1) of <10 pptv for a 1-min integration period and <4 pptv for a 5-min integration period (in adverse field sampling conditions). These detection limits are expected to be improved from threefold to fivefold for modest system improvements involving increases in the number of PMTs (4 vs 1) and the use of moderately higher photolysis (30-mJ/pulse) and probe laser (5-mJ/pulse) energies.

The VUV/PF-LIF technique is inherently linear over more than 5 orders of magnitude change in NH_3 concentration. Optical pre/post filtering nonlinear effects have been shown, as expected, not to occur for concentrations below ppmv levels. However, as currently configured, the gated photon counting electronics suffer from multiple photons per gate being counted as one pulse (also known as pulse pile-up).[46] At this time, diffusive optical attenuators, placed in front of the PMT, have been used to maintain electronic counting linearity into ranges that nominally cover hundredfold changes in NH_3 concentration. Figure 5 shows a typical calibration curve obtained over the range of 100–13,000 pptv. The correlation coefficient of the least-squares fit of this data set is 0.997. Gated

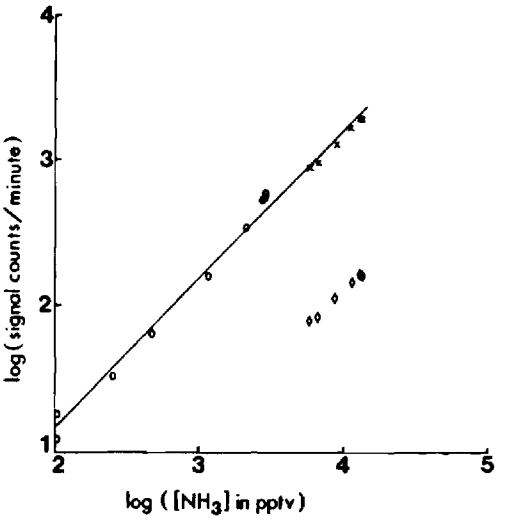

Fig. 5. Calibration curve of the UV-PF-LIF ammonia sensor: ○, count rates measured with signal attenuation with one diffuser; ◇, count rates measured with three diffusers; ×, count rates of the three diffuser data multiplied by the change in increased attenuation (11.6×).

analog signal processing techniques are currently available that would eliminate the limited dynamic range of the gated photon counting system used in the present instrument.

For NH_3 concentrations significantly above the LOD, the measurement precision of the instrument is dominated by the photon statistical fluctuations in the observed signal count rate [e.g., (observed NH_3 signal counts)$^{1/2}$]. For a nominal instrument sensitivity of 1.5 photons/pptv/min, the measurement uncertainties at the 95% confidence limit (2σ) for NH_3 concentrations of 30, 100, and 200 pptv, and integration times of 1 min, would be ±30%, ±16%, and ±12%, respectively. The uncertainty associated with normalizing laser performance via the observed reference cell signal would add $\leq \pm 6\%$ (2σ) uncertainty (for a factor of 2 change in instrument sensitivity). The uncertainty associated with the water vapor $NH(b^1\Sigma^+)$ deactivation correction would be $< \pm 18\%$ (2σ) (in worst-case conditions of 10-Torr change in $[H_2O]$). For more typical changes in water vapor of ±2 Torr, the uncertainty, from this effect, would be $\leq \pm 6\%$ (2σ).

The absolute calibration accuracy has been estimated to be $\leq \pm 18\%$ (at the 95% confidence limit) based on intercomparison of numerous certified NH_3 standards and the combined uncertainties in the calibration and sample mass flow measurements.

Typical spike response times, using a high flow rate 8-m inlet manifold system, are shown in Figs. 6(a) and (b). A 4-m inlet system exhibited an average rise (10–90%) time of 5 min and average fall time (90–10%) of 3 min. Similar tests on an 8-m inlet system demonstrated an average 90–10% decay time of 5 min. Of primary importance to remote atmospheric applications is the memory associated at low NH_3 concentration ($[NH_3] <$ 100 pptv). Observations using ambient air and $^{15}NH_3$ as a tracer gas showed decay of the observed signal from $^{15}NH_3$ approach baseline levels with a $1/e$ fall time constant of 3^{+2}_{-1} min over a wide range of ambient temperatures and relative humidity for an 8-m inlet system at 1200 slpm (0.8-s residence time).

In the UV/PF-LIF method, no atmospheric compound can produce a positive signal unless the following three criteria are satisfied for the spectrally interfering species produced from the parent atmospheric compound: (1) it must be produced in air by 193-nm photolysis of the parent compound, (2) it must survive the delay between the photolysis and probe laser pulses, and (3) it must fluoresce within the 326-nm emission filter passband when excited by the narrowband probe laser tuned to a specific $NH(b^1\Sigma^+ \Rightarrow c^1\Pi)$ rovibronic absorption line at 452 nm. Because of these stringent requirements, it is believed that only those compounds which produce the $NH(b^1\Sigma^+)$ radical through 193-nm photolysis can be considered as potential interferences. In particular, the most likely interfering species might be the organic amines: monomethylamine (NH_2CH_3), dimethylamine [$NH(CH_3)_2$], and monoethylamine ($NH_2C_2H_5$). The fluorescence signals produced by each of these amines were compared to that resulting from an equivalent NH_3 concentration in air. These results are summarized in Table I. Trimethylamine [$N(CH_3)_3$] was also included in these tests as a check of the consistency of the approach since no NH fragment was expected in its photolysis. Although hydrazine (N_2H_4) and HN_3 are known to produce NH when photolyzed at 193 nm,[50,51] neither of these compounds is predicted to be present in the atmosphere at significant levels compared to NH_3 (Ref. 7) and therefore are not included in the test.

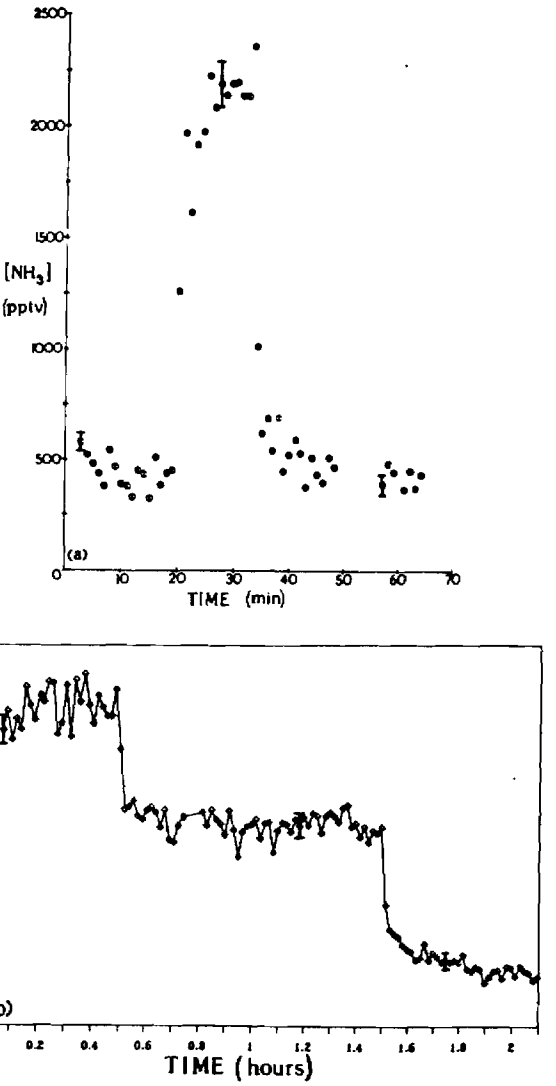

Fig. 6. (a) Temporal response of 1800-pptv addition to ambient air. (b) Low level step function additions of ammonia; representative error bars are shown for the 1σ measurement precision for each representative concentration.

As is apparent from Table I, trimethylamine, as expected, produced no detectable signal, while the other amines tested all yielded a concentration normalized signal 6–10% as strong as that from ammonia. In the case of monomethylamine the result was consistent with estimates of the impurity level of NH_3 in the sample. However, both dimethylamine and monoeth-

Table I. Relative Fluorescence Signal Strengths for Various Potentially Interfering Species

Compound	Relative signal[1]
NH_3	100
NH_2CH_3	7 ± 2
$NH(CH_3)_2$	10 ± 10
$N(CH_3)_3$	0 ± 1
$NH_2C_2H_5$	6 ± 4

[1] Relative signal refers to signal level observed for a test compound relative to the signal observed for an equal concentration of NH_3.

ylamine appeared to give signal levels in excess over what was anticipated using vendor specified levels of impurities. At this time, the resolution of the question as to the impact of these results on the selectivity of this method appears to be academic, since the atmospheric levels of amines are predicted to all be well below the level of NH_3 in the troposphere. Hence, no significant interference by these compounds is anticipated.

Tests were also conducted to assess if any non-NH containing compounds produced a measurable spectral interference. In excess of 10 h of total measurement time was dedicated, in a variety of atmospheric conditions, to monitoring the net signal obtained when the probe laser is tuned-off of a $NH(b^1\Sigma^+) \Rightarrow NH(c^1\Pi)$ transition, and no net signal above the statistical uncertainty in the 193-nm generated background counts has ever been observed.

Laser decomposition of ammonia containing aerosols has been suggested as a possible interference mechanism for the VUV/PF-LIF technique. Direct assessment of this potential source of interference has been complicated by the associated high levels of gas phase NH_3 present in equilibrium with liquid or dry aerosols containing ammonia compounds. Based on recent investigations into the mechanisms for laser initiated aerosol decomposition[52-55] it is reasonably safe to assume that, for the laser irradiation conditions used in our system (i.e., Δt = 8 ns, 0.03 J/cm^2, λ = 193 nm, $I = 3.8 \times 10^6$ W/cm^2), optical breakdown will not occur even in conditions of high aerosol loading. Furthermore, aerosol decomposition resulting in an observable signal [i.e., aerosol $\Rightarrow NH_3$ (gas) $\Rightarrow NH(b^1\Sigma^+)$] must occur during the 8-ns, 193-nm photolysis laser pulse, since the sample cell residence time is less than the time between laser pulses. For the laser conditions given above it should also be safe to assume that liquid aerosols (with or without a solid core) will not volatilize appreciable NH_3 (gas) during the 8-ns photolysis laser pulse duration, since the laser fluence is below the superheat limit for aqueous aerosols $\geq$0.4-μm diameter (even for highly absorbing liquid aerosols).

At this time it appears as though the only possible interference from laser decomposition of aerosols might occur from small dry aerosols with diameters $\leq$0.4 μm for which the aerosol mass is sufficiently small to allow temperature rises of >25°C/ns. Worst-case conditions can be described by (1) the first half of the laser pulse (4 ns) is effectively used to form NH_3 in the gas phase [e.g., NH_4NO_3 (s) $\Rightarrow NH_3$ (gas) + HNO_3 (gas)], (2) the second half of the laser pulse is used to form the $NH(b^1\Sigma^+)$ state from the sublimated NH_3 (gas), and (3) sublimation/decomposition is instantaneous. In these conditions, which probably would not occur as sublimation/decomposition is most likely not instantaneous on the nanosecond time scale, the 193-nm laser pulse could conceivably generate 5×10^7 NH_3 molecules for total decomposition of the 0.2-μm NH_4NO_3 aerosol. The second half of the 193-nm laser pulse could then photolyze this NH_3 component with the efficiency equal to that for ambient NH_3, thereby yielding an equivalent interference of 2.5×10^7 NH_3 molecules per aerosol particle. However, even at sonic velocity, the expanding decomposition products, NH_3 (gas) + HNO_3 (gas), will yield number densities of NH_3 and HNO_3 within the localized area of the decomposed aerosol that ranges from $\sim 10^{22}$ to $\sim 10^{16}$ molecules/cm^3 over the time range from 10 ns to 1 μs. These large localized number densities would greatly increase the quenching rate experienced by $NH(b^1\Sigma^+)$ radicals within the expanding vapor cloud, resulting in 1/e quenching times ranging from 0.25 ns to 25 μs as the vapor cloud expands. Therefore, very little of the $NH(b^1\Sigma^+)$ state population formed is expected to survive the time delay between the photolysis and probe laser pulses (i.e., 2–10 μs) as $\gg$10 (1/e) decay times should be experienced over this time range.

Interferences from laser decomposition of either aqueous or dry ammonia containing aerosols are estimated to yield $\leq$100-pptv equivalent NH_3 ambient gas phase concentration for severe pollution episodes in which the ammonia aerosol concentration is as high as 33-μg NH_4^+/m^3 (i.e., 46 ppbv). In these conditions, however, the NH_3 ambient gas phase equilibrium concentration is expected to be >1 ppbv over the temperature range of 200–350 K.

The photolysis laser pulse will photodissociate not only NH_3 but also numerous other atmospheric compounds (namely, O_2, O_3, HNO_3, CS_2, etc.), producing a number of highly reactive atomic and radical species (namely, O^1D, OH, CS, etc.), as well as the H atoms formed from the photolysis of ammonia. Reactions involving these photolytically produced species are not viewed as a problem since even for near collision frequency limited reaction rates (i.e., $k \simeq 2 \times 10^{-10}$ cm^3/molec s) and concentrations as high as 1×10^{14} molec/cm^3, no significant perturbation of the $NH(b^1\Sigma^+)$ population is expected for 2 μs < t_d < 10 μs. Photodissociation of water and oxygen, the most abundant atmospheric compounds dissociated at 193 nm, have exhibited little effect on this technique other than that expected for the quenching of the $NH(b^1\Sigma^+)$ state by the parent molecules.[46] Mass transport out of the photolysis/sample cell eliminates any possible complications due to secondary chemistry (residence time <0.1 s) although the effect of secondary chemistry has been observed in slow flow or sealed systems.

As a final note, the VUV/PF-LIF sensor has recently

participated in an NH_3 instrument intercomparison (Jan.–Mar. 1989, Boulder, CO). The results of this intercomparison will be published elsewhere.[34] Due to the data/publication protocol, which has been established for intercomparison participants, details of the results cannot be provided as of this writing. However, a summary of several important test results conducted by our group during unofficial intercomparison time periods are worth noting at this time. During ambient sampling periods in which relative humidities varied from 10% to 90%, no statistically significant loss in observed VUV/PF-LIF signal strength was found (i.e., $\Delta D_{\lambda_3} \leq \pm 10\%$) using $^{15}NH_3$ as a tracer gas. The effects of inlet long term memory on the measurement of low ambient NH_3 concentrations (i.e., <500 pptv) were examined through sample flow rate changes (300–2400 slpm), sample inlet line cleaning and heating tests, and $^{15}NH_3$ tracer tests. Only the sample line heating test exhibited a statistically significant variation in the observed NH_3 signal, which is believed to be due to the decomposition of NH_3 containing aerosols.

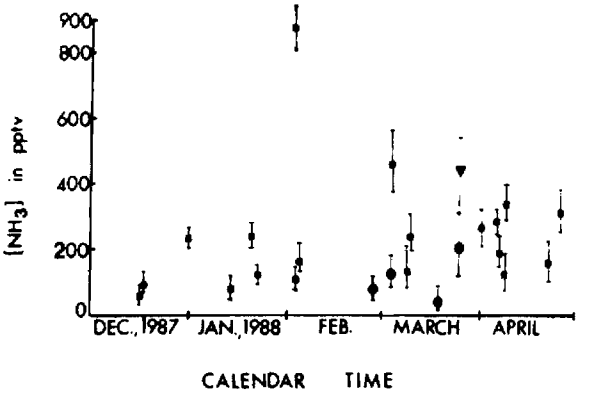

Fig. 7. Plot of the concentration of NH_3 vs calendar time for the period of Dec. 1987 through Apr. 1988. All the measurements were made at the Stone Mountain field site. Each data point represents the average [NH_3] measured during the time periods (▼) 0:0–8:00 GMT, (●) 8:00–16:00 GMT, (■) 16:00–24:00 GMT, with arrows indicating the minimum and maximum values observed in the measurement period.

III. Field Measurements and Observations

During the fall 1987 and winter/spring 1988, VUV/PF-LIF field measurements of ammonia were conducted at Georgia Tech's Stone Mountain field sampling facility. This facility is located atop Stone Mountain, which is ~17 miles east of downtown Atlanta. The sampling facility occupies the sixth floor of a 7- × 7- × 30-m (high) tower that has an elevation of 520-m MSL, 250 m above the surrounding terrain, and 20 m above the surface of the mountaintop.

Unique aspects of the Stone Mountain field site include (1) its height above the surrounding terrain makes it reasonably insensitive to the effects of localized sources, even though it is located on the edge of suburban Atlanta; (2) the height of the mountain allows for frequent encounters with clouds when frontal systems pass through north central Georgia (this situation provided an opportunity to further assess the importance of aerosol scavenging in controlling NH_3 levels in a clear air mixed-cloud environment); and (3) the elevation of the sampling site is such that at night the top of the nocturnal boundary layer typically sets up at a height that is below the top of the mountain where in these conditions the levels of trace gases encountered are often more typical of rural lower free tropospheric air than they are of suburban or urban Atlanta air. Overall, the Stone Mountain field site has been found to be a very interesting one from a scientific point of view, offering a wide variety of atmospheric sampling conditions.

The program to study tropospheric NH_3 at the Stone Mountain field site has centered around testing the sensor in a variety of ambient sampling conditions and examining the seasonal variation in the levels of ammonia. Toward these goals, the ammonia instrument was operated for ~3 weeks during the early fall of 1987, and again from the middle of Dec. 1987 through the end of Apr. 1988. Most of the present discussion focuses on this later grouping of experiments as the fall measurements primarily focused on system testing. During the period from Dec. 1987 through Apr. 1988 data were taken over the course of 24 separate days, during mostly daylight hours from late morning to early evening (e.g., 16:00–23:00 GMT). Several measurement periods of longer duration were also made to study the diurnal variation in ammonia. Meteorological parameters that were routinely measured and recorded during the periods of ammonia measurement included: temperature, pressure, dew point, wind speed, wind direction, UV and visible solar flux, and synoptic weather data for the southeastern U.S.A. received from the National Weather Service.

A summary of the data taken during the winter–spring period is shown in Fig. 7. While limited, this data set does indicate a distinct, albeit slight, increase in the average ammonia levels observed as the winter changed into spring. Preliminary work performed at Stone Mountain in the early fall of 1987 exhibited NH_3 levels that ranged between 1000 and 3000 pptv (average 1500 pptv), well above the highest concentrations measured the following winter and spring. This suggests a trend in which NH_3 levels, observed at Stone Mountain, are lowest during the winter months and are highest during the hotter summer or early fall months. The high NH_3 levels of the fall previous to the winter and spring of 1988 also suggest that the slight upward trend observed in Fig. 7 should have increased as spring entered into summer. This hypothesis supports the observation of increasing NH_3 levels from spring to summer[56,57] that were attributed to elevated surface soil temperature. However, these observations appear to contradict the observation of a spring maximum with somewhat lower levels of NH_3 being observed during the summer months.[58] The spring maximum was believed to be due to the impact of heavy applications of ammonium nitrate fertilizer to nearby farmland. Any apparent discrepancy among

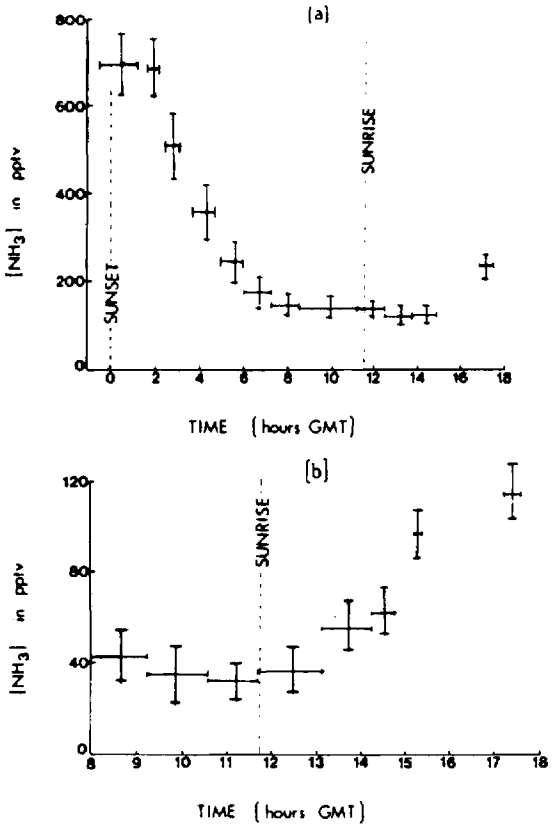

Fig. 8. Plots of the concentration of NH_3 vs time for the measurements of $[NH_3]$ at the Stone Mountain field site. Each horizontal bar in the graphs indicates the average NH_3 level recorded within the period included and vertical bars represent minimum/maximum values over the period averaged. (a) Results of the measurements made from sunset 22 Mar. 1988 to noon 23 Mar. 1988. The weather was clear but with increasing cloudiness occurring on the morning of 23 Mar. The average temperature was 10.5°C with 56% relative humidity. (b) Results of the measurements made from ~4 h before sunrise to noon 17 Mar. 1988. The weather was clear. The average temperature was −1.5°C with 42% relative humidity.

these observations most likely reflects the differences in soil types, land utilization practices, and the extent of anthropogenic perturbations at the various field sites.

Significant diurnal variations in ambient ammonia concentration were also observed at the Stone Mountain sampling site as shown in Fig. 8. It is believed that this diurnal variation is due to a capping-off of the nocturnal boundary layer at an elevation below that of the sampling site as evidenced by boundary layer heights estimated from the inversion layer height viewed over nearby Atlanta. The approximate four-fold elevation in NH_3 concentrations shown in Fig. 8(b) closely followed visual observations of the break-up in the nocturnal boundary layer through the early morning hours.

Figures 8(a) and (b) are intended to show the differences in NH_3 levels between nighttime and daytime for the winter season at Stone Mountain. They are also intended to illustrate the potential relationship between the localized measured concentration of NH_3 atop Stone Mountain and observations of related parameters (such as nocturnal boundary layer). However, these data should not necessarily be considered as the norm for this season, as only four diurnal measurements were performed during the winter and spring of 1988. Certainly more data collection is necessary before definitive conclusions can be drawn.

To estimate the effect air temperature had on the levels of NH_3 between days of cloud/rain events and days of relatively clear weather, the data were broken up into four categories according to both air temperature (AT) and relative humidity (RH) level: data at <5°C AT and <50% RH, data at <5°C AT and ≥50% RH, data ≥5°C AT and <50% RH, and data at ≥5°C AT and ≥50% RH. Within each category, the average concentration of ammonia was calculated as presented in Table II.

The results in Table II certainly cannot be considered conclusive since they represent a rather limited data set and no attempt has been made to decouple the seasonal trend in the data, which may be due to elevated temperatures and changes in fertilizer usage or both, from the results of Table II. However, some features of the results are worth noting. For example, comparing all the data of <5°C air temperature with the data of ≥5°C air temperature, a marked temperature effect is seen: an ~2.5-fold increase in NH_3 concentrations on going from cold days to relatively warm days. Separating the data further, by relative humidity, within each of the two temperature ranges, provides some information on the effect relative humidity has on NH_3 concentrations. For the data of <5°C air temperature, on days when the relative humidity was ≥50%, the average NH_3 concentration was not statistically different from the day when the relative humidity was <50%. The difference in the average NH_3 concentration between the high and low relative humidity data sets for the data of ≥5°C air temperature exhibits a similar trend in that the average NH_3 concentration for the high humidity days is not statistically different from the low humidity days. And, of the high humidity days, over half of the data represent measurements taken during periods when low lying stratus clouds were sampled. The highest concentration of gas phase ammonia measured during the winter/spring of 1988, 877 pptv, was measured while sampling dense clouds, near 100% relative humidity and intermittent rain or drizzle.

While soil moisture and temperature changes can certainly have significant impacts on ammonia emission rates, as will fertilizer application practices in suburban regions preceding frontal passages, it is believed that these measurements sharply contrast those made by Force *et al.*[19] In this latter study gas phase ammonia was observed to dramatically decrease as the relative humidity increased past 50% even though the deliquescence point for NH_4NO_3 aerosols lies at >60% relative humidity. The authors hypothesized that the decrease in observed NH_3 (gas) was due to liquid phase aerosol scavenging. An alternative explanation of

Table II. Comparison of Daily Average NH_3 Concentrations with Meteorological Conditions for Measurements Made at the Stone Mountain Field Site from Dec. 1987 to Apr. 1988 (Observed Between 16:00 and 20:00 GMT)

Date	Temperature °C	Relative humidity	Weather conditions	$[NH_3]$ in pptv
Category one:	<5°C, <50% relative humidity			
3/17/88	−1.5	42	Clear, cold	114
			Avg:	114
Category two:	<5°C, ≥50% relative humidity			
12/16/87	−3.0	77	Clear, cold	59
12/17/87	−1.0	60	Clear, cold	94
1/13/88	0.0	78	Clear, getting cold	85
1/21/88	2.0	93	Cloudy, cold	116
2/26/88	−1.5	80	Clear, cold	160
			Avg: 104 ± 34	(1σ)
Category three:	≥5°C, <50% relative humidity			
12/31/87	15.2	35	Cloudy, getting colder	241
3/2/88	15.0	27	Clear	227
3/7/88	17.5	38	Clear/hazy, warm	138
3/8/88	18.0	37	Cloudy, warm	246
3/30/88	21.0	47	Cloudy, warm	266
4/5/88	26.5	25	Clear/hazy, hot	291
4/6/88	13.0	41	Clear, high winds	189
4/7/88	11.0	33	Clear, windy	127
4/8/88	18.5	41	Clear/hazy	340
4/25/88	20.0	42	Clear/partly cloudy	310
			Avg: 238 ± 60	(1σ)
Category four:	≥5°C, ≥50% relative humidity			
1/19/88	11.0	82	LLSS,[a] some rain, warm	236
2/2/88	13.0	100	LLSS, rain/drizzle, warm	877
2/3/88	18.0	85	LLSS, warm	108
2/4/88	7.5	87	Partly cloudy, clearing, getting colder	163
3/3/88	18.0	60	Cloudy, LLSS and drizzle, warm	455
4/21/88	18.0	50	Clear	161
			Avg: 333 ± 270	(1σ)
			Avg(w/o 2/2/88) 224 ± 122	(1σ)

[a] LLSS refers to sampling of low lying stratus clouds.

their data set is that the surface emission rate increased substantially over the 10–15.5°C change in ambient air temperature. This coupled with stronger vertical mixing velocities that should have been experienced later in the day (10:30–12:00 EDT vs 14:00–16:00 EDT) could account for the observed change in NH_3 concentrations. However, neither the above explanation nor the one offered by Force *et al.*[19] lends support to the accusation made by Langford *et al.*[33] that hydration of ammonia may further limit the usefulness of highly specific spectroscopic techniques.

It is also interesting to note that on both days shown in Fig. 8 the relative humdity was >50% before sunrise and <50% as the boundary layer height (and subsequent temperature) rose through the morning. On the surface this appears as the same trend seen by Force *et al.*[19] However, we believe that the increase in ammonia as the RH dropped (i.e., temperature increased) is due to changes in boundary layer height (and the associated increased coupling with soil emissions) rather than to a lowering of the relative humidity.

To date, significant depletion of gas phase NH_3 by aerosols, fog, or cloud processes has only been observed by our group on one occasion that involved sampling of ice particle laden air during the winter 1989 Boulder Intercomparison Field Program (detailed results to be reported elsewhere). Artifact gas phase ammonia produced by aerosol decomposition on the sample inlet line cannot be absolutely ruled out as a source of the observed ammonia signals, in cloud sampling conditions. Artifact ammonia is, however, not believed to significantly contribute to the observed signal due to the short residence time (<1 s) and near ambient pressure/temperature conditions within the sample manifold system. Obviously, more detailed studies of the particle and aqueous phase equilibrium of ambient NH_3 containing aerosols and droplets and subsequent heterogeneous removal via rain/washout are needed, especially in view of the large uncertainty associated with NH_3 sticking coefficients on naturally occurring atmospheric aerosol surfaces over the temperature range of 230–315 K.

IV. Conclusions

A VUV/PF-LIF sensor has been developed and tested that is capable of making routine measurements of gas phase atmospheric ammonia in the few parts-per-trillion-by-volume range (i.e., 10 pptv = 2.5×10^8 molec/cm^3 at 1 atm pressure). Current limits of detection (LOD) (for a S/N = 2/1) are <10 pptv for a 1-minute signal integration period, and <4 pptv for a 5-min signal integration period in moderate aerosol loadings and high ambient water vapor conditions. For clean air sampling, more typical of the remote troposphere, the instrument LOD is expected to improve slightly to <5 and <2 pptv for 1- and 5-min integration times, respectively. While they have not proved necessary to date, modest instrument improvements should easily result in limits of detection of <2 and <1 pptv for 1- and 5-min integration periods in clean remote free tropospheric sampling conditions.

The spectral selectivity of the technique allows for calibration and tracer studies using either $^{15}NH_3$ or $^{14}NH_3$ as the specifically monitored trace gas. This aspect should provide unique opportunities over other currently available techniques in the study of NH_3 phase equilibria with atmospheric aerosols and droplets.

As yet no interferences, either gas phase or aerosol phase, have been identified as being significant in atmospheric sampling conditions. In addition, the instrument performance is not degraded in adverse sampling conditions (i.e., rain, fog, clouds, haze, etc.).

The VUV/PF-LIF instrument can be configured for operation on an aircraft platform, as has been demonstrated with similar LIF systems developed by our group that have now logged over 500 h of total airborne measurement time for the measurement of the molecules OH,[59] NO,[49] and NO_2.[36] There are no inherent

36. S. T. Sandholm, J. D. Bradshaw, K. S. Doris, M. O. Rodgers, and D. D. Davis, "An Airborne Compatible Photofragmentation Two-Photon Laser Induced Fluorescence Instrument for Measurements of Atmospheric $NO/NO_x/NO_2$," J. Geophys. Res. J. Geophys. Res. **95**, 10,155–10,162 (1990).
37. J. B. Halpern, W. M. Jackson, and V. McCrary, "Multiphoton Sequential Photodissociative Excitation: a New Method of Remote Atmospheric Sensing," Appl. Opt. **18**, 590–592 (1979).
38. T. Ni, S. Yu, X. Ma, and F. Kang, "$NH(A^3\Pi \rightarrow X^3\Sigma^-)$ Emission from 193 nm Two-Photon Photolysis of NH_3," Chem. Phys. Lett. **126**, 413–416 (1986).
39. V. M. Donnelly, A. P. Baronavski, and J. R. McDonald, "ArF Laser Photodissociation of NH_3 at 193 nm: Internal Energy Distributions in $NH_2\tilde{X}^2B$, $\tilde{A}^2A_1$, and Two-Photon Generation of NH $A^3\Pi$ and $b^1\Sigma^+$," Chem. Phys. **43**, 271–281 (1979).
40. H. K. Haak and F. Stuhl, "ArF Excimer Laser Photolysis of Ammonia. Formation of NH and ND in the $A^3\Pi$ State," J. Phys. Chem. **88**, 2201–2204 (1984).
41. R. D. Kenner, F. Rohrer, and F. Stuhl, "Generation of $NH(a^1\Delta)$ in the 193 nm Photolysis of Ammonia," J. Chem. Phys. **86**, 2036–2043 (1987).
42. R. D. Kenner, F. Rohrer, R. K. Browaryik, A. Kaes, and F. Stuhl, "Two-Photon Formation of $NH/ND(A^3\Pi)$ in the 193 nm Photolysis of Ammonia. I. Mechanism and Identification of the Intermediate Species," Chem. Phys. **118**, 141–152 (1987).
43. J. D. Bradshaw, M. O. Rodgers, and D. D. Davis, "Single Photon Laser-Induced Fluorescence Detection of NO and SO_2 for Atmospheric Conditions of Composition and Pressure," Appl. Opt. **14**, 2493–2500 (1982).
44. J. D. Bradshaw, M. O. Rodgers, and D. D. Davis, "Sequential Two-Photon Laser-Induced Fluorescence: a New Technique for Detecting Hydroxyl Radicals," Appl. Opt. **23**, 2134–2145 (1984).
45. M. O. Rodgers, K. Asai, and D. D. Davis, "Photofragmentation-Laser Induced Fluorescence: a New Method for Detecting Atmospheric Trace Gases," Appl. Opt. **19**, 3597–3605 (1980).
46. C. A. vanDijk, S. T. Sandholm, D. D. Davis, and J. D. Bradshaw, "$NH(b^1\Sigma^+)$ Deactivation/Reaction Rate Constants for the Collisional Gases H_2, CH_4, C_2H_6, Ar, N_2, O_2, H_2O and CO_2," J. Phys. Chem. **93**, 6363–6367 (1989).
47. F. Rohrer and F. Stuhl, "Collision-Induced Intersystem Crossing $NH(c'\Pi) \rightarrow NH(A^3\Pi)$," J. Chem. Phys. **86**, 226–233 (1987).
48. G. L. Hutchinson, U.S.D.A. Agricultural Research Service, Fort Collins, CO 80552; private communication.
49. J. D. Bradshaw, M. O. Rodgers, S. T. Sandholm, S. KeShang, and D. D. Davis, "A Two-Photon Laser-Induced Fluorescence Field Instrument for Ground-Based and Airborne Measurements of Atmospheric NO," J. Geophys. Res. **90**, 12861–12873 (1985).
50. H. K. Haak and F. Stuhl, "ArF (193 nm) Laser Photolysis of HN_3, CH_3NH_2, and N_2H_4: Formation of Excited NH Radicals," J. Phys. Chem. **88**, 3627–3633 (1984).
51. H. Okabe, "Photodissociation of HN_3 in the Vacuum-Ultraviolet Production and Reactivity of Electronically Excited NH," J. Chem. Phys. **49**, 2726–2733 (1968).
52. R. G. Pinnick, A. Biswas, R. L. Armstrong, S. G. Jennings, J. D. Pendleton, and G. Fernández, "Micron-Sized Droplets Irradiated with a Pulsed CO_2 Laser: Measurements of Explosion and Breakdown Thresholds," Appl. Opt. **29**, 910–925 (1990).
53. W.-F. Hsieh, J.-B. Zheng, C. F. Wood, B. T. Chu, and R. K. Chang, "Propagation Velocity of Laser-Induced Plasma Inside and Outside a Transparent Droplet," Opt. Lett. **12**, 576–578 (1987).
54. B.-S. Park and R. L. Armstrong, "Laser Heating of Droplets with Absorbing Core," Appl. Opt. **29**, 334–336 (1990).
55. B.-S. Park, A. Biswas, R. L. Armstrong, and R. G. Pinnick, "Delay of Explosive Vaporization in Pulsed Laser-Heated Droplets," Opt. Lett. **15**, 206–208 (1990).
56. H. W. Georgii and W. J. Müller, "On the Distribution of Ammonia in the Middle and Lower Troposphere," Tellus **26**, 180–184 (1974).
57. N. Yamamoto, N. Kabeya, M. Onodera, S. Takahahi, Y. Komori, E. Nakazuka, and T. Shirah, "Seasonal Variation of Atmospheric Ammonia and Particulate Ammonia Concentrations in the Urban Atmosphere of Yokohama over a 5-Year Period," Atmos. Environ. **22**, 2621–2623 (1988).
58. J. S. Levine, T. R. Augustsson, and J. M. Hoell, "The Vertical Distribution of Tropospheric Ammonia," Geophys. Res. Lett. **7**, 317–320 (1980).
59. M. O. Rodgers, J. D. Bradshaw, S. T. Sandholm, S. KeSheng, and D. D. Davis, "A 2-λ Laser-Induced Fluorescence Field Instrument for Ground-Based and Airborne Measurements of Atmospheric OH," J. Geophys. Res. **90**, 12819–12824 (1985).

Reprinted from The Journal of Physical Chemistry, 1989, 93, 6363.

$NH(b^1\Sigma^+)$ Deactivation/Reaction Rate Constants for the Collisional Gases H_2, CH_4, C_2H_6, Ar, N_2, O_2, H_2O, and CO_2

C. A. van Dijk, S. T. Sandholm, D. D. Davis, and J. D. Bradshaw*

School of Geophysical Sciences, Georgia Institute of Technology, Atlanta, Georgia 30332
(Received: August 2, 1988; In Final Form: January 20, 1989)

The $NH(b^1\Sigma^+)$ radical was produced via two-photon photodissociation of NH_3 by use of an ArF excimer laser. Detection of this radical species was achieved by laser pumping the transition $NH(b^1\Sigma^+) \rightarrow NH(c^1\Pi)$ at 452 nm followed by fluorescence monitoring of the $NH(c^1\Pi) \rightarrow NH(a^1\Delta)$ transition at 326 nm. Deactivation/reaction rate constants for the process $NH(b^1\Sigma^+) + M \rightarrow$ products were measured for the following collisional gases: Ar, N_2, O_2, CO_2, H_2O, H_2, CH_4, and C_2H_6. The measured rate constants ranged from 7.1×10^{-17} to 1.0×10^{-12} cm^3/(molecule-s) for deactivation/reaction by Ar and H_2O, respectively.

Introduction

As one of the prominent trace gas species in the atmosphere, there has been an increasing interest in the atmospheric chemistry of ammonia. Much of this interest has been the result of the major role this species plays in controlling the acidity of precipitation.[1-5] For this reason, considerable effort has been expended over the past decade to develop reliable methods for detecting NH_3 under atmospheric conditions. One of these new detection methodologies has involved the photofragmentation of the NH_3 species by using 193-nm radiation from an ArF excimer laser.[6] This new method involves the monitoring of the NH_3 photolysis product, $NH(b^1\Sigma^+)$. The latter radical species, which has been shown to arise from a two-photon-dissociation process in NH_3,[7] has the advantage of being metastable. Its reported radiative lifetime is 53 ms.[8] Thus, laser pumping the $NH(b^1\Sigma^+)$ species to the $NH(c^1\Pi)$ level can be sufficiently delayed (e.g., 2 μs) as to permit several 1/e decay times of the background fluorescence produced from the 193-nm photolysis laser. However, since the $NH(b^1\Sigma^+)$ species may also be deactivated via collision with atmospheric gases, critical to estimating the sensitivity of the latter NH_3 detection method are the deactivation/reaction rate coefficients for $NH(b^1\Sigma^+)$ with representative atmospheric gases.

Presented here are the results from a study that has examined the rate coefficients for the deactivation/reaction of the $NH(b^1\Sigma^+)$ radical in the presence of various possible atmospheric gases, including both major constituents as well as several of the more prominent minor gases.

Experimental Section

As described by Schendel et al.,[6] the photolytic scheme used in this study to generate and detect the $NH(b^1\Sigma^+)$ species is summarized below and in the energy level diagram depicted in Figure 1.

$$NH_3 + 2h\nu_1 \xrightarrow{\lambda_1 = 193\ nm} NH(b^1\Sigma^+) + \text{products} \quad (1)$$

$$NH(b^1\Sigma^+) + h\nu_2 \xrightarrow{\lambda_2 = 452\ nm} NH(c^1\Pi) \quad (2)$$

$$NH(c^1\Pi) \xrightarrow{\lambda_3 = 326\ nm} NH(a^1\Delta) + h\nu_3 \quad (3)$$

The detailed nature of the two-photon-generated $NH(b^1\Sigma^+)$ species from NH_3 is still not fully understood but is believed to involve the initial formation of the $NH_2(A)$ state and/or highly vibrationally excited NH_2, e.g., reactions 4 and 5 and/or 6 and 7. Energetically, the formation of the $NH(b^1\Sigma^+)$ radical requires

$$NH_3 + h\nu_1 \xrightarrow{\lambda = 193\ nm} NH_2(A) + H \quad (4)$$

$$NH_2(A) + h\nu_1 \xrightarrow{\lambda = 193\ nm} NH(b^1\Sigma^+) + H \quad (5)$$

$$NH_3 + h\nu_1 \xrightarrow{\lambda = 193\ nm} NH_2^* + H \quad (6)$$

$$NH_2^* + h\nu_1 \xrightarrow{\lambda = 193\ nm} NH(b^1\Sigma^+) + H \quad (7)$$

the absorption of two 193-nm photons, a conclusion that was verified in this work with the observation of an approximate square power dependence in the production of the $NH(b^1\Sigma^+)$ species as a function of the 193-nm laser fluence (i.e., plot of log fluorescence vs log 193-nm energy yielded a slope of 1.7 ± 0.3 over the energy range of 3–30 mJ/cm^2).[6] A plot of the rotational level distribution versus energy, using the appropriate Honl–London expression[9] and level spacing and rotational constant[10] yielded a $NH(b^1\Sigma^+)$

* Author to whom correspondence should be addressed.

(1) National Research Council. *Sulfur Oxides*; National Academy of Sciences Press: Washington, DC, 1978.
(2) National Research Council. *Acid Deposition*; National Academy of Sciences Press: Washington, DC, 1983.
(3) National Research Council. *Global Tropospheric Chemistry*; National Academy of Sciences Press: Washington, DC, 1984.
(4) Charlson, R. J.; Chameides, W. L.; Kley, D. *The Biogeochemical Cycling of Sulfur and Nitrogen in the Remote* Atmosphere; Galloway, J. N., Charlson, M. O., Andreae, M. O., Rodhe, H., Eds.; Reidel: Boston, 1985.
(5) Calvert, J. G.; Stockwell, W. R. *Environ. Sci. Technol.* **1983**, *17*, 428A.
(6) Schendel, J.; Stickel, R.; van Dijk, C.; Sandholm, S.; Bradshaw, J.; Davis, D. *J. Atmos. Chem.* To be submitted for publication.
(7) Donnelly, V. M.; Baronavski, A. P.; McDonald, J. R. *Chem. Phys.* **1979**, *43*, 271.
(8) Blumenstein, U.; Rohrer, F.; Stuhl, F. *Chem. Phys. Lett.* **1984**, *107*, 347.
(9) Herzberg, G. *Spectra of Diatomic Molecules*; Van Nostrand Reinhold: New York, 1970.

0022-3654/89/2093-6363$01.50/0

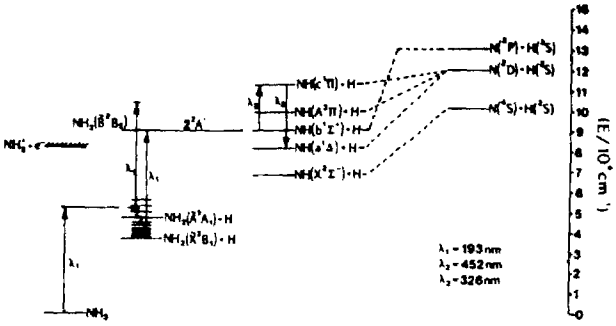

Figure 1. Energy level diagram depicting the photolysis of $NH_3 + h\nu_1 \rightarrow NH_2 + h\nu_1 \rightarrow NH(b^1\Sigma^+)$ at $\lambda_1 = 193$ nm followed by laser-induced probing of the $NH(b^1\Sigma^+, v''=0)$ state at $\lambda_2 = 452$ nm via the $NH(b^1\Sigma^+) + h\nu_2 \rightarrow NH(c^1\Pi)$ transition with the resultant fluorescence monitored near $\lambda_3 = 326$ nm corresponding to the $NH(c^1\Pi) \rightarrow NH(a^1\Delta) + h\nu_3$ transition.

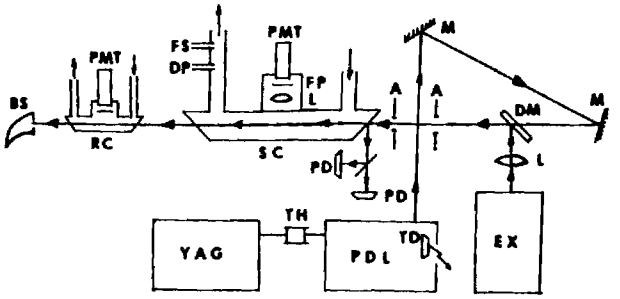

Figure 2. Schematic figure of the PF-LIF NH_3 detection system: A, aperture; BS, beam stop; DM dichroic mirror; DP, dew-point hygrometer; EX, ArF excimer laser; FP, band-pass filter; L, lens; M, mirror; PD, photodiode; PDL, pulsed dye laser; PMT, photomultiplier tube; RC, reference cell; SC, main sampling cell; TD, trigger diode; TH, third-harmonic generator; YAG, Nd:YAG laser.

average temperature of 293 (±5) K. There were no significant deviations of any levels from a Boltzmann distribution when monitored 2 μs after the photoflash at a total pressure of 760 Torr of Ar or 760 Torr of synthetic air.

Figure 2 shows a schematic representation of the photofragmentation laser-induced fluorescence (PF-LIF) system used in this study. As noted already, the photolysis laser consisted of an ArF excimer system having an average energy output of ~12 mJ/pulse, which when apertured to a 5-mm diameter produced an ~2.4 mJ/pulse photolysis beam with a pulse width of ~8 ns.

The tunable 452-nm laser beam used to pump the $NH(b^1\Sigma^+)$ species into the $NH(c^1\Pi)$ state was generated by using the third harmonic from a Nd:YAG laser to drive an oscillator/amplifier dye laser. This system as well as the excimer laser were nominally operated at 10 Hz. The dye laser output wavelength was typically centered near 452 nm having an output energy of ~1 mJ/pulse with a line width of ~0.2 cm^{-1}. The 452-nm probe laser beam was expanded to ~1.5-cm diameter and then apertured to a 10-mm diameter. This configuration allowed the (~0.4 mJ) 10-mm-diameter probe beam to encompass the 5-mm-diameter excimer photolysis beam. To obtain deactivation/reaction rate decay data for the process

$$NH(b^1\Sigma^+) + M \rightarrow \text{products} \qquad (8)$$

a time delay was imposed between the photolysis laser and the 452-nm probe laser. The minimum time delay utilized in these experiments (i.e., 2 μs) was sufficient to allow for not only the room temperature thermalization within the $NH(b^1\Sigma^+)$ state but also the complete decay of any nascent $NH(c^1\Pi)$ population that might be formed via the 193-nm photolysis laser. The available time delays typically allowed for the observation of 2–3 1/e decay times in the concentration level of the $NH(b^1\Sigma^+)$ species. Other experimental details involving the photofragmentation/laser-induced fluorescence $NH_3/NH(b^1\Sigma^+)$ detection system will be given elsewhere;[6] thus, only a brief overview of these details is provided below.

The laser initiated fluorescence (i.e., λ = 326 nm) from the $NH(c^1\Pi) \rightarrow NH(a^1\Delta)$ transition was detected with a Hamamatsu R331 photomultiplier tube after passage through a 326-nm narrow band-pass optical filter. Collection of the 326-nm fluorescence was achieved by using f 1.4 collection optics. The pulse counting electronics used in conjunction with the fluorescence monitoring PMT have been described previously.[11] The observed signal counts were corrected for the probability of multiple photons being observed by the photomultiplier, yet only being counted as a single event by the gated photon counter according to the expression

$$C_{cor} = C_{max}\left[\ln\left(1 - \frac{C_{obsd}}{C_{max}}\right)\right] \qquad (9)$$

where C_{max} is the maximum possible count (i.e., number of gate events per integration period) and C_{obsd} is the observed signal count per integration period. This correction to the observed signal count has been shown to be valid for $C_{obsd}/C_{max} \leq 0.67$, a value that was not exceeded in these experiments.[6,12]

In addition, it was necessary to gate off the photomultiplier photocathode for a period of ~1 μs surrounding the 193-nm photolysis laser pulse in order to keep the photomultiplier tube from becoming saturated by scatter and/or fluorescence produced by the 193-nm photolysis laser.

As shown in Figure 2, a unique feature of the PF-LIF detection system used in this study involved the use of a $NH_3/NH(b^1\Sigma^+)$ reference fluorescence cell. The signal from this cell was used to establish the optimum wavelength for pumping the $NH(b^1\Sigma^+)$ radical and for monitoring both the photolysis and probe laser performance throughout a given set of kinetic experiments.

Because of the elevated signal level, the output from the reference cell was sampled in the analogue mode using a gated-charge-integrator. Linearity in the 326-nm fluorescence signal $NH(c^1\Pi) \rightarrow NH(a^1\Delta)$ was demonstrated for NH_3 concentration levels ranging over 5 orders of magnitude.

During a given data run involving the deactivation/reaction of the $NH(b^1\Sigma^+)$ species, the performance of the PF-LIF system typically changed less than 20%. As a further precaution in minimizing any systematic errors resulting from changes in laser performance, for each delay time selected three to five independent runs were carried out. These independent runs were staggered in time such that short delay time runs were alternated with long delay time runs, a run being defined as the average value obtained from three to five 1- or 2-min-integration periods. Data was normalized for laser drift by linearly extrapolating the performance characteristics to a designated time delay (e.g., 2 μs), a delay time that was measured several times in each data run. This method of normalization was chosen since the reference cell normalization can not be extrapolated to other time delays owing to its individual $NH(b^1\Sigma^+)$ deactivation environment.

Throughout this study experimental conditions were maintained such that the decay in the concentration level of the $NH(b^1\Sigma^+)$ species occurred under pseudo-first-order conditions (i.e., for the process $NH(b^1\Sigma^+) + M \rightarrow$ products (8), $[M] \gg [NH(b^1\Sigma^+)]$). Considering the short 1/e decay times measured for all gases investigated in this study (i.e., <1 ms), diffusion losses of the NH species were small compared to the deactivation/reaction process. Corrections to the measured first-order rate coefficients due to diffusion effects should be <1% for the probe/photolysis laser beam geometries used in this experiment (i.e., the probe laser beam has 2-fold larger diameter than the photolysis laser).

To minimize chamber wall memory problems as well as the possibility of secondary reactions in this study, both involving NH_3 as well as added deactivation/reactant gases or products, all experiments reported in this study were performed under con-

(10) Whittaker, F. L. *J. Phys. B (Proc. Phys. Chem. Soc.)* **1978**, *2*, 977.

(11) Bradshaw, J.; Rodgers, M. O.; Sandholm, S.; KeSheng, S.; Davis, D. D. *J. Geophys. Res.* **1985**, *90*, 12, 861.

(12) Crannell, H.; Danforth, D. *Nucl. Instrum. Methods* **1967**, *55*, 372.

TABLE I: Rate Coefficients for the Deactivation/Reaction of $NH(b^1\Sigma^+, v' = 0)$[a]

collisional gas species	k value, $cm^3/(molecule \cdot s)$		
	this work[b]	ref 14[c]	ref 16[d]
H_2O	$(1.0 \pm 0.21) \times 10^{-12}$	$(4.9 \pm 1.5) \times 10^{-13}$	
H_2	$(4.5 \pm 2.1) \times 10^{-13}$	$(8.6 \pm 2.6) \times 10^{-13}$	$(1.0 \pm 0.24) \times 10^{-12}$
CH_4	$(8.5 \pm 1.5) \times 10^{-14}$	$(1.8 \pm 0.5) \times 10^{-13}$	
C_2H_6	$(2.6 \pm 0.6) \times 10^{-13}$		
CO_2	$(1.5 \pm 0.6) \times 10^{-14}$	$<1 \times 10^{-14}$	
N_2	$(5.3 \pm 1.2) \times 10^{-16}$	$(6.0 \pm 0.6) \times 10^{-16}$	$(4.48 \pm 0.6) \times 10^{-16}$
O_2	$(2.0 \pm 0.6) \times 10^{-15}$	$(2.4 \pm 0.7) \times 10^{-15}$	$(2.44 \pm 2.5) \times 10^{-16}$
Ar	$(7.1 \pm 0.6) \times 10^{-17}$	1.8×10^{-16}	$(1.27 \pm 0.12) \times 10^{-16}$ $(1.61 \pm 0.18) \times 10^{-16}$

[a] All uncertainties given at 99% confidence level (3σ) based on stated measured precisions. [b] Total estimated uncertainty $\leq \pm 37\%$ for gases H_2O, N_2, C_2H_6, and CH_4 and $\leq \pm 60\%$ for the gases Ar, H_2, O_2, and CO_2 (all at the 99% confidence limit). [c] Total estimated uncertainty stated to be $\leq \pm 30\%$ for the gases H_2O, H_2, CH_4, CO_2, N_2, and O_2 and $\geq \pm 30\%$ for Ar (all at the 99% confidence limit). [d] Uncertainties taken from 65% confidence limit uncertainties reported; no statement as to estimated total uncertainty was given.

tinuous-flow conditions. Typical flow rates in these experiments ranged from 70 to 200 L/min, yielding residence times from 1.1 to 0.4 s, respectively. To achieve the desired concentrations of NH_3, diluent gas, and deactivating gas, a continuous flow serial dilution system using calibrated mass-flow meters was employed. The addition of deactivation/reactant gases, [M], was accomplished via dilution with an appropriate diluent gas. The concentration of these gases was expressed as a ratio of mass flow rates. This ratio of mass-flow rates had a maximum uncertainty of $<\pm 5\%$.

The NH_3 gas employed in this study was Scott Specialty made up as a certified standard in N_2 at a concentration level of 100 ppmv (2.5×10^{15} molecules/cm^3 at 1 atm total pressure). Distilled H_2O was purchased from Burdick and Jackson. The latter gas was introduced into the main gas flow line by diverting a fraction of the total flow through an H_2O bubbler. The concentration of H_2O in the final gas stream was determined by UV absorption measurements and by using a General Eastern two-stage dew-point hygrometer. The latter device was also employed in determining the H_2O level in ambient air samples, an alternate approach that was employed to assess the deactivation of the $NH(b^1\Sigma^+)$ species via collision with H_2O. The uncertainty in $[H_2O]$ is estimated to be $\leq \pm 10\%$ over the range of water vapor used in these experiments.

The gases H_2, CH_4, C_2H_6, and CO_2 were ultra-high-purity grade and used without further purification, whereas, O_2, N_2, and Ar were obtained from the boil-off of their respective liquids. All gases were used without further purification.

An assessment of secondary chemical effects in this study involving H atoms, HN_2, NH_2*, $NH_2(A)$, or H_2 from the photolysis of NH_3 has shown that at the estimated concentration levels for the above species (i.e., for $[NH_3] \leq 5 \times 10^{11}/cm^3$ and $[H_xN_y] \leq 10^{11}/cm^3$) their influence on the measured k values for process 8 should have been negligibly small. For example, even with the assumption of unit collision efficiency, the 1/e reaction time of $NH(b^1\Sigma^+)$ with the above species is calculted to be nearly 2 orders of magnitude larger than that for process 8. Similarly, deactivation of $NH(b^1\Sigma^+)$ arising from secondary reactions initiated by products of the primary processes being studied (e.g., CH_3 in the case of M = CH_4, OH in the case of M = H_2O) should have also been negligible owing to the low NH_3 concentrations used in this study. The concentration of these radical species was less than $[NH(b^1\Sigma^+)]$ (i.e. $\leq 10^{11}/cm^3$). The possibility of secondary reactions arising from species formed from the photolysis of added atmospheric gases is discussed later in the text. Tests involving variations in the 193-nm laser fluence by factors of 3–5 further confirmed the absence of any major kinetic complications when M was N_2, H_2O, or Ar. In addition, tests in which the laser repetition rate was varied from 2 to 10 pps also confirmed a lack of product buildup within the flow system when M was H_2O. In all cases straight-line plots of ln fluorescence vs time were observed.

A final consideration in assessing the reliability of these data involved possible kinetic complications resulting from our monitoring the $NH(c^1\Pi)$ species rather than $NH(b^1\Sigma^+)$. In this case since the deactivation/reaction times for the $NH(c^1\Pi)$ species

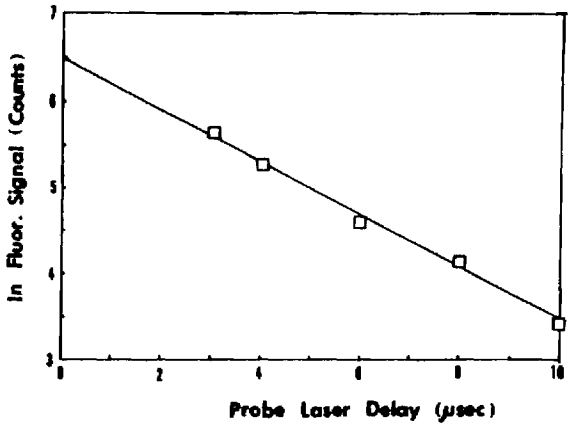

Figure 3. Ln fluorescence signal (counts) versus time (probe laser delay time) for the process $NH(b^1\Sigma) + H_2O \rightarrow$ products. $[H_2O] = 8$ Torr in ambient air at 760 Torr; $[NH_3] = 2.3 \times 10^{11}$ molecules/cm^3.

under the conditions employed in our experiments were in the range of nanoseconds to subnanoseconds,[13] compared to the microsecond to millisecond times for $NH(b^1\Sigma^+)$, no deconvolution of the measured decay curves arising from this effect was required.

Results and Discussion

The first-order-decay times for each gas were obtained from a least-squares fit of the data, i.e., natural logarithm of the fluorescence intensity versus probe laser delay time for a constant collision partner mixture. In this manner deactivation of the $NH(c^1\Pi)$ state from which fluorescence was observed occurred on time scales $\ll 0.1$ μs for the 1 atm buffer gases used here. Thus the effects of $NH(c^1\Pi)$ quenching on the analysis of $NH(b^1\Sigma^+)$ lifetime measurements were inconsequential, affecting only the magnitude of the observed $NH(c^1\Pi) \rightarrow NH(a^1\Delta)$ fluorescence and not the probed $NH(b^1\Sigma^+)$ lifetime.

Bimolecular rate coefficients were obtained from the slope of first-order decay plots (ln fluorescence intensity versus probe laser delay time) and the concentration of deactivation/reactant gas. These values were corrected for the decay rate contributed by the buffer gas used. The stated uncertainties in these bimolecular rate coefficients were calculated from the probable error in the slope taken from a linear regression analysis. The values reported correspond to the mean values obtained from the various partial pressures utilized where the uncertainty is taken from the combined uncertainty in the independent measurements (i.e., $\sigma^2_{total} = \sum \sigma^2_i/(n-1)$) and are expressed at the 65% confidence limit (i.e., 1σ). The associated uncertainty in deconvoluting the buffer gas contribution is taken into account quadratically.

Representative first-order-decay plots for Ar, N_2, N_2O, H_2, CH_4, and C_2H_6 are shown in Figures 3–5. Modified Stern–Volmer plots for the collision gas partners H_2O and O_2 are shown in Figures 6 and 7. These results are listed in Table I along with

(13) Rohrer, F.; Stuhl, F. *J. Chem. Phys.* **1987**, *86*, 226.

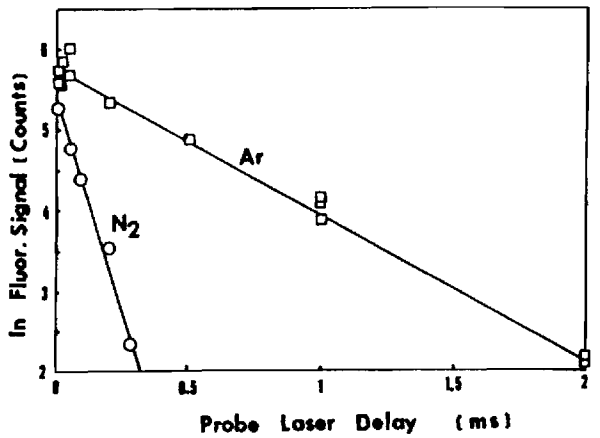

Figure 4. Ln fluorescence signal (counts) versus time (probe laser delay time) for the processes $NH(b^1\Sigma) + N_2$, Ar → products. [Ar] = 760 Torr; $[N_2]$ = 760 Torr; $[NH_3] = (0.8–1.6) \times 10^{11}$ molecules/cm^3.

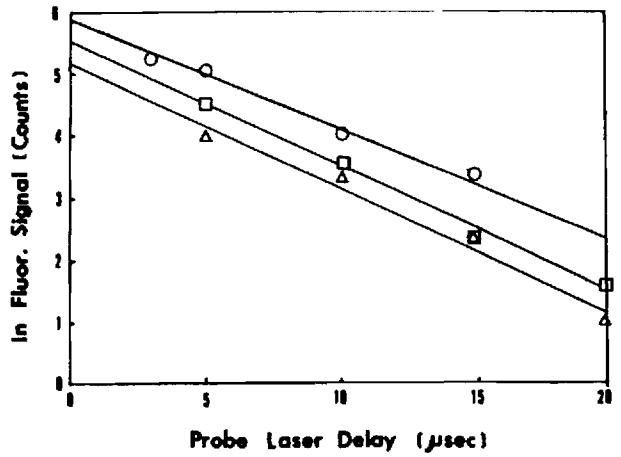

Figure 5. Ln fluorescence signal (counts) versus time (probe laser delay time) for the processes $NH(b^1\Sigma) + H_2$, CH_3, and C_2H_6 → products. (□) $[H_2]$ = 12 Torr in 760 Torr of N_2; (○) $[CH_4]$ = 62 Torr in 760 Torr of N_2; (△) $[C_2H_6]$ = 20.5 Torr in 760 Torr of N_2; $[NH_3] = (2.0–4.3) \times 10^{11}$ molecules/cm^3.

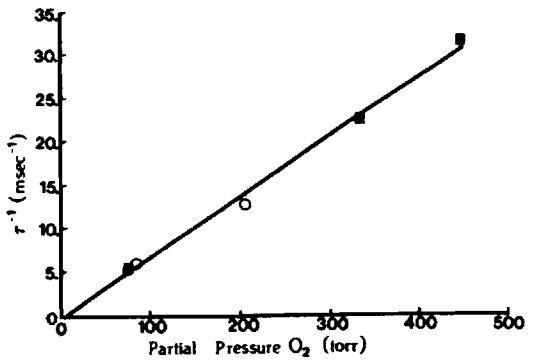

Figure 6. Reciprocal lifetime (s^{-1}) versus partial pressure of O_2 in 760 Torr mixtures of Ar (○) and N_2 (■).

those of other investigators whose data are taken at low total pressure.

For the gases N_2 and Ar, only the deactivation process (10) should occur:

$$NH(b^1\Sigma^+) + N_2, Ar \rightarrow NH(a^1\Delta) \text{ and/or } NH(X^3\Sigma) \qquad (10)$$

The measured deactivation rates for these two gases were $(5.3 \pm 0.4) \times 10^{-16}$ and $(7.1 \pm 0.2) \times 10^{-17}$ cm^3/(molecules·s), respectively. Rate constants were measured for collider partial pressures of 760 Torr in the case of Ar and at 198, 274, and 760 Torr in the case of N_2 with Ar as a buffer gas.

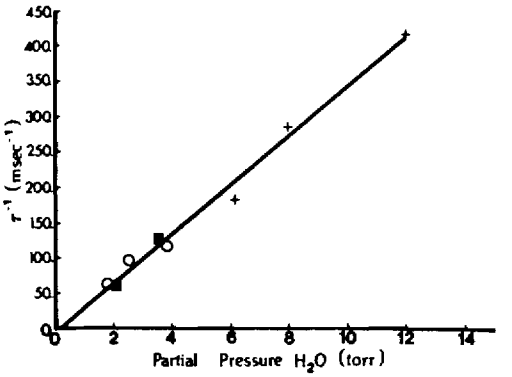

Figure 7. Reciprocal lifetime (s^{-1}) versus partial pressure of H_2O in 760 Torr mixtures of N_2 (■), artificial air (○), and ambient air (+).

The latter k values are the smallest values measured of all collisional gases examined and very likely reflect a combination of factors such as the lower polarizability of these two gases and the absence of chemical reaction channels. The difference between N_2 and Ar may reflect both the higher polarizability of N_2 vs Ar as well as the availability of internal energy levels in the case of N_2.

A comparison of our results with other reported values (see Table I) shows excellent agreement for the case of N_2 and, within the stated uncertainties, acceptable agreement for the gas Ar.

CO_2 and O_2. For the gases CO_2 and O_2 in addition to the deactivation channel (10), the possibility exists for chemical reactions to occur. One of these chemical reaction channels might involve the formation of the HNO species as a product, e.g.

$$NH(b^1\Sigma^+) + CO_2 \rightarrow HNO + CO \qquad \Delta H_{r_1} = -52 \text{ kcal/mol} \qquad (11)$$

$$NH(b^1\Sigma^+) + O_2 \rightarrow HNO + O \qquad \Delta H_{r_2} = -60 \text{ kcal/mol} \qquad (12)$$

The exothermicity of both (11) and (12) would suggest the potential importance of these reaction pathways.

The k values measured for CO_2 and O_2 were $(1.5 \pm 0.2) \times 10^{-14}$ and $(2.0 \pm 0.2) \times 10^{-15}$ cm^3/(molecule·s), respectively. These k values are approximately 1–2 orders of magnitude greater than those measured for N_2 and Ar where only the deactivation channel was available. Collider partial pressures were 105 Torr for CO_2 and ranged between 76 and 448 Torr for O_2 as shown in Figure 6. The buffer gas was N_2 for the CO_2 case and N_2 or Ar for the O_2 case. In addition, our measured rate constant for a 25% O_2 artificial air mixture of $(9.4 \pm 0.5) \times 10^{-16}$ cm^3/(molecule·s) is in good agreement with that calculated from our individual rate constants for N_2 and O_2 (i.e., $(9.0 \pm 0.6) \times 10^{-16}$ cm^3/(molecule·s)).

A comparison of our k values for CO_2 and O_2 with other reported values shows reasonable agreement for both species within the specified uncertainties for each set of measurements.

Kinetic complications in our measurements of the k values for CO_2 and O_2 appear to be minimal to nonexistent. In the case of CO_2, the direct photolysis of CO_2 by the 193-nm excimer would have produced $<1.4 \times 10^{13}$ O atoms/cm^3 at the highest CO_2 concentration utilized assuming a quantum yield of unity and taking the absorption cross section from Okabe.[15] Thus, even with the assumption that O atoms reacted with $NH(b^1\Sigma^+)$ at gas kinetic collision efficiency (i.e., $k \sim 4 \times 10^{-10}$ cm^3/molecule) the calculated $1/e$ decay time would have been 180 μs. This can be compared to our measured value of 20 μs. Similarly for O_2, the estimated yield of O atoms from the 193-nm photolysis of O_2 would have produced $<4 \times 10^{15}$ O atoms/cm^3 (for O_2 at 448 Torr

(14) Zetzsch, C.; Stuhl, F. *Ber. Bunsen-Ges. Phys. Chem.* **1976**, *80*, 1354.

(15) Okabe, H. *Photochemistry of Small Molecules*, Wiley-Interscience: New York, 1978.

(16) Gelernt, B.; Filseth, S.; Carrington, T. *Chem. Phys. Lett.* **1975**, *36*, 238; *J. Chem. Phys.* **1976**, *65*, 4940.

and unit quantum efficiency). Under the experimental conditions of our system, however, these O atoms would have reacted with O_2 to form O_3

$$O + O_2 + M \rightarrow O_3 + O_2 \quad (13)$$

with a 1/e time of ~4 μs. Thus, the more important concern might be reaction of O_3 with the NH($b^1\Sigma^+$) species. Assuming a rate coefficient of 10^{-12} cm³/(molecule·s), which is the largest k value measured for any species in this study (e.g., H_2O), the estimated 1/e time for deactivation/reaction with O_3 is 280 μs. This can be compared to a measured 1/e time of 31 μs. It is to be noted also that no statistically significant change in the value of k_2 was observed with a variation in the O_2 concentration of approximately a factor of 6.

H_2, CH_4, C_2H_6, and H_2O. As in the case of CO_2 and O_2, in addition to the deactivation channel (10), the possibility exists for reaction of the above species with NH($b^1\Sigma^+$). One possible reaction channel for each of these species is

$$NH(b^1\Sigma^+) + H_2 \rightarrow NH_2 + H \qquad \Delta H_{r_{14}} = -51 \text{ kcal/mol} \quad (14)$$

$$NH(b^1\Sigma^+) + CH_4 \rightarrow NH_2 + CH_3 \qquad \Delta H_{r_{15}} = -51 \text{ kcal/mol} \quad (15)$$

$$NH(b^1\Sigma^+) + C_2H_6 \rightarrow NH_2 + C_2H_5 \qquad \Delta H_{r_{16}} = -50 \text{ kcal/mol} \quad (16)$$

$$NH(b^1\Sigma^+) + H_2O \rightarrow NH_2 + OH \qquad \Delta H_{r_{17}} = -35 \text{ kcal/mol} \quad (17)$$

As noted above, energetically, each of the above reactions could occur as well as possible others.

The k values measured for the gases H_2, CH_4, C_2H_6, and H_2O were $(4.5 \pm 0.7) \times 10^{-13}$, $(8.5 \pm 0.5) \times 10^{-14}$, $(2.6 \pm 0.2) \times 10^{-13}$, and $(1.00 \pm 0.07) \times 10^{-12}$ cm³/(molecule·s), respectively. Rate constants were measured at collider partial pressures of 12.1, 24.3, and 57.0 Torr in the case of H_2, at 46.7 and 62.3 Torr in the case of CH_4, and at 20.7, 21.9, and 38.6 Torr in the case of C_2H_6, all of which utilized N_2 as a buffer gas. Rate constants were measured for H_2O vapor ranging from 1.95 to 11.9 Torr using both N_2 and air as a buffer gas (see Figure 7). Again, it can be seen that the k values for these gases, which may both react with or deactivate NH($b^1\Sigma^+$) upon collision, are 2–3 orders of magnitude greater than those for N_2 and Ar, where only channel 10 is possible. The authors note also that, in the case of H_2O, similar k_{H_2O} values were obtained for the diluent gases, N_2, synthetic air, and ambient air.

A comparison of our results with other reported values shows only fair agreement, within the stated error limits of each study, for the gases H_2 and CH_4 and H_2O. In the case of H_2O, our value is approximately a factor of 2 greater than that reported by Zetzsch and Stuhl, a difference that exceeds the stated uncertainties of each study. One possible explanation for this difference may involve the reliability of the measured H_2O level used in Zetzsch and Stuhl's experiment. In their study a static gas fill system was employed. Thus, considering the high degree of wall loss of H_2O, the actual H_2O concentration may have been lower than what they estimated from their static pressure measurements. As discussed earlier in the text, the present study used a dynamic flow configuration which allowed for the rapid equilibration of H_2O between the gas phase and the walls. Still an alternative explanation might involve a possible third-body effect.[13] In the Zetzsch and Stuhl study very low pressures (few Torr) were used, whereas in this study near atmospheric pressures were employed. In the case of H_2 and CH_4 our values are approximately 2-fold lower than those reported by Gelernt et al. and Zetzsch and Stuhl. One possible explanation could be secondary reactions involving either CH_3 radicals or H atoms which may have built up in the static systems used in the latter study.[8]

Kinetic complications in the measurement of the k values for H_2, CH_4, and C_2H_6 are estimated to be negligibly small due to the minimal absorption by these gases at 193 nm. In the case of H_2O, the maximum production of OH ($<10^{14}$ molecules/cm³ assuming an absorption cross section $\leq 2.5 \times 10^{-20}$ cm² and unit quantum yield) would have resulted in an estimated 1/e decay time of ~25 μs, assuming the reaction with NH($b^1\Sigma^+$) occurred on every collision (i.e., $k \sim 4 \times 10^{-10}$ cm³/molecule). Our measured 1/e time was ~2.5 μs.

As stated previously, the uncertainties listed in the text correspond to the measurement precision at the 65% confidence level (i.e., 1σ). The uncertainty in these measurements did not exceed ±22% at the 99% confidence limit (3σ) for the colliders H_2O, N_2, air, C_2H_6, and CH_4. In addition, our estimated uncertainty in collision partner concentration, time base, and other experimental factors should be <±15%. Our estimated combined total uncertainty for the values reported here is ≤±37% at the 99% (3σ) confidence limit for these gases. For the colliders Ar, H_2, O_2, and CO_2 this estimate is somewhat higher and should be taken at ≤±60%.

Although the absolute sensitivity of the vacuum-UV/photofragmentation laser-induced fluorescence (vacuum-UV/PF-LIF) NH_3 detection methodology depends inversely on the quenching of the upper excited ($c^1\Pi$) state, the sensitivity of this method, as well as other LIF methods, has been shown to be independent of pressure when given in terms of signal strength per unit concentration when the concentration is expressed as a mixing ratio (i.e., parts per trillion by volume, pptv).[6,11] This is true in the case of fluorescence arising from the NH($c^1\Pi$) state as O_2 dominates quenching of this state compared to N_2 or H_2O. For photolysis to probe laser delay times greater than 1 μs and from the above set of measurements, it now appears as though water vapor will be the most important gas that will impact on the detection limit/sensitivity of the vacuum-UV/PF-LIF method owing to water vapor's highly varying atmospheric mixing ratio and its rapid deactivation/reaction rate coefficient for the NH($b^1\Sigma^+$) state.

Acknowledgment. We acknowledge the support of this research by the National Science Foundation under Grant ATM8610236.

Registry No. NH, 13774-92-0; H_2O, 7732-18-5; H_2, 1333-74-0; CH_4, 74-82-8; C_2H_6, 74-84-0; CO_2, 124-38-9; N_2, 7727-37-9; O_2, 7782-44-7; Ar, 7440-37-1.